et al., 1997]. HCV genotype is an important predictor of response to interferon-alpha and ribavirin combination therapy [Hnatyszyn, 2005]. The route of transmission and serological reactivity are other factors which may differ among different HCV genotypes [Dhaliwal et al., 1996]. However, it is unclear, whether or not HCV genotypes differ in their pathogenicity [Zein, 2000].

One hundred seventy million people worldwide estimated to be infected with HCV are at a risk of developing progressive liver disease and death due to infection with HCV [WHO, 1999]. According to different reports, the prevalence of HCV in Egypt ranges from 11% to 14% of the general population, with 5–7 million people with active infection (have detectable HCV RNA) [Abdel-Wahab et al., 1994; Arthur et al., 1997; Abdel-Aziz et al., 2000]. By these estimates, Egypt is considered to be the country with the highest prevalence rate of HCV in the world with a majority of genotype 4 [Frank et al., 2000].

Few data are available regarding the molecular epidemiology of HCV in south Egypt. The aim of this study was to extend the mid-core and NS5B database for HCV strains isolated from HCV-infected patients residing in south Egypt with respect to the clinical and virological characteristics of the isolates examined.

PATIENTS AND METHODS

Patients

Serum samples were collected from August to October 2007 from 151 consecutive chronic liver disease patients seen in affiliated hospitals of Sohag University Hospital and South Egypt Cancer Institute. Among the 151 patients with hepatitis, 30 were assigned into asymptomatic carrier group, 86 into a liver cirrhosis group, and 35 into an HCC group. Anti-HCV was detected in a total of 126/151 (83.4%); 25/30 (83.3%) in the asymptomatic carrier group, 68/86 (79.1%) in the liver cirrhosis group, and 33/35 (94.3%) in the HCC group. In addition to the specimens collected consecutively, sera were collected also from 41 patients with diagnosed chronic hepatitis C. The clinical classification of the patients infected with HCV was based upon (1) measurement of serum alanine aminotransferase (ALT), (2) ultrasound examination, and (3) detection of a serological tumor marker (alpha fetoprotein for the diagnosis of HCC). The asymptomatic carrier group include patients with anti-HCV with normal liver enzymes for more than 6 months with minimal or no symptoms. Patients with liver cirrhosis were diagnosed clinically by the presence of splenomegaly, ascites, and other peripheral signs of portal hypertension together with ultrasonographic findings such as a shrunken, coarse texture liver with enlarged portal and splenic veins. A total of 167 anti-HCV-positive samples belonged to patients from three governates in south Egypt, 93 samples from the Sohag governate (467 km from Cairo), 45 samples from the Assuit governate (375 km south of Cairo), and 29 samples from the Qena governate (600 km south of Cairo).

Serological Methods

Serum samples were examined for anti-HCV, hepatitis B surface antigen, anti-HBc, and anti-HBs by chemiluminescence enzyme immunoassay using commercial assay kits (Fujirebio, Inc., Tokyo, Japan). Hepatitis C core antigen (HCVcAg) was measured using enzyme immunoassay (Fujirebio, Inc.) [Aoyagi et al., 1999].

Detection of the HCV RNA

Viral RNA extraction was carried out with a Sepa-Gean RV-RN Nucleic acid extracting kit (Sanko Junyaku Co. Ltd., Tokyo, Japan) following the manufacturer's protocol. The extracted RNA was reverse transcribed into cDNA using SuperScript II RNAse H Reverse Transriptase (Invitrogen Corp., Carlsbad, CA) and random hexamer primers (Takara Shuzo, Co. Ltd., Tokyo, Japan) as described previously [Ohno et al., 1997]. Confirmation of HCV RNA was performed by amplifying partial genome of the 5-non-coding region according to the protocol described previously [Takeuchi et al., 1999].

Sequencing and Phylogenetic Analysis

For genotyping the HCV isolates, PCR was used to amplify parts of both the structural (core/E1) and non-structural (NS5B) coding regions of the HCV [Tanaka et al., 2002]. The sequencing reaction of the amplified products was performed with the Prism Big Dye (Pekrin-Elmer Applied Biosystems, Foster City, CA) in an ABI 3100 DNA automated sequencer according to the manufacturer's protocol. Sequences were aligned with the CLUSAL X software program [Thompson et al., 1994]. The phylogenetic trees were constructed by neighbor joining method with Tamura-Nei distance correction model using online tools in the HCV database [Shin-I et al., 2008]. Bootstrap values were determined on 1,000 resampling tests in the HCV database. The sequences of other HCV isolates used for the phylogenetic analysis were retrieved from the DDBJ/EMBL/GenBank sequence database and are indicated by their accession number in the phylogenetic tree. The nucleotide sequence data reported in this article will appear in the DDBJ/EMBL/GenBank sequence databases with accession numbers: AB470005–AB470069, AB470243–AB470255, and AB470103–AB470215. Statistical analysis was performed with Fisher's exact probability test and an independent *t*-test for continuous variables using the SPSS software package (SPSS, Chicago, IL). *P*-values (two-tailed) less than 0.05 were considered statistically significant.

RESULTS

Demographic and Clinical Characteristics of the Patients With Chronic Liver Disease

Figure 1 summarizes the detected rates of hepatitis markers and coinfection patterns among the clinical

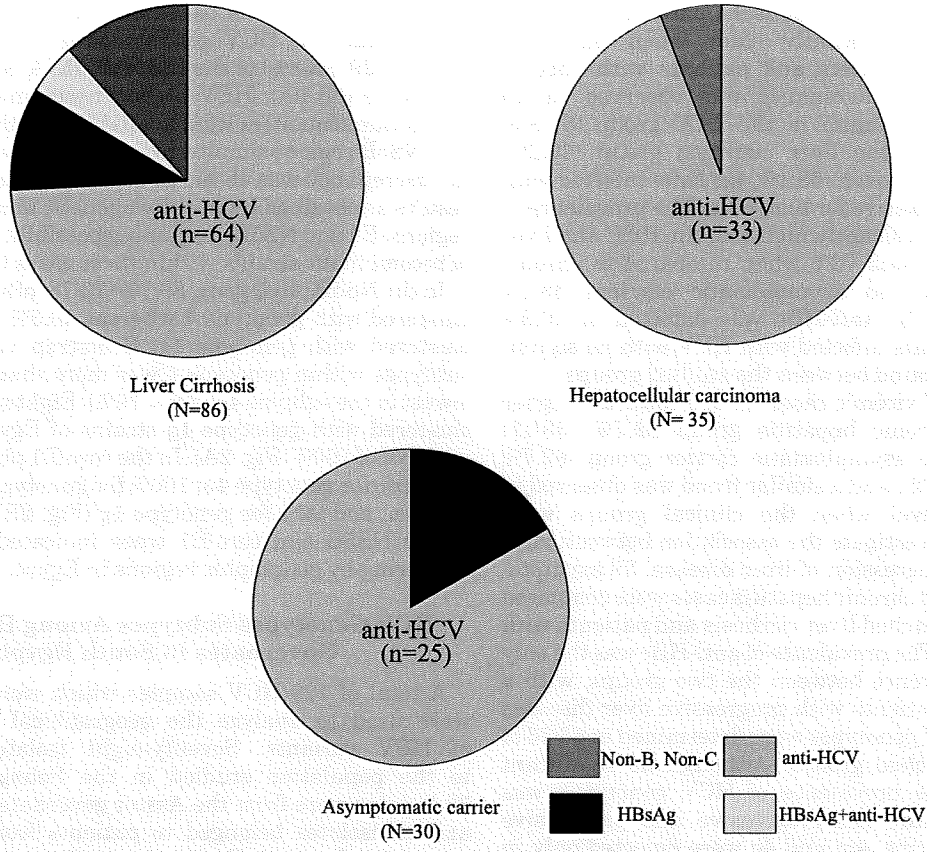

Fig. 1. Incidence of hepatitis markers among patients with progressive liver diseases.

groups studied; asymptomatic carriers (n = 30), liver cirrhosis (n = 86), and HCC (n = 35). Anti-HCV and HBsAg were detected in 25/30 (83.3%) and 5/30 (16.7%) of the asymptomatic carriers, respectively. In the liver cirrhosis group, anti-HCV was detected in 64/86 (74.4%), HBsAg was detected in 8/86 (9.3%), and simultaneous presence of both markers was detected in 4/86 (4.7%). Ten patients (11.6%) in the liver cirrhosis group were negative serologically for both anti-HCV and HBsAg and were designated as non-B hepatitis and non-C hepatitis, respectively. In the HCC group, anti-HCV was detected in 33/35 (94.3%), whereas the remaining two patients (5.7%) were negative for both anti-HCV and HBsAg and were designated as non-B hepatitis and non-C hepatitis.

Table I summarizes the baseline features of the 167 patients infected with HCV subdivided into four clinical groups: 25 asymptomatic carriers, 41 chronic hepatitis, 68 liver cirrhosis, and 33 patients with HCC. Patients in the HCC group were older than patients in

TABLE I. Description of the Patients Infected With HCV Stratified by Their Clinical Characteristics

	Total (n = 167)	Asymptomatic carrier (n = 25)	Chronic hepatitis (n = 41)	Liver cirrhosis (n = 68)	HCC (n = 33)	*P* value
Age[a]	47.5 ± 11.8	29.8 ± 7.0*	43.4 ± 6.7	52.5 ± 7.8	59.0 ± 8.6*	<0.006
Gender (male)	116 (69.4)	16 (64)	32 (78)	41 (60.2)	27 (81.8)	NS
ALT (IU/L)[a]	42.7 ± 28.5	28.4 ± 16.2*	42.3 ± 17.1	42.8 ± 29.6	70.8 ± 42.1*	<0.005
AST (IU/L)[a]	64.9 ± 46.0	29.6 ± 9.8*	63.5 ± 34.2	75.4 ± 53.8	86.1 ± 47.2*	<0.0001
HCVcAg (fmol/L)[b]	434.2 (0.1–19,654)	463 (0.1–12,549.8)	1,162.5 (5.0–19,654)	409.6 (0.1–13,219.2)	741.6 (50.7–7,703.8)	NS
HCV RNA[c]	139 (83.2)	19 (76)	38 (92.7)	56 (82.4)	26 (78.8)	NS
HBsAg[c]	5 (3.0)	0	1 (2.4)	4 (5.9)	0	NS
Anti-HBs[c]	33 (19.8)	6 (24)	9 (22)	10 (24.4)	8 (24.2)	NS
Anti-HBc[c]	97 (58.1)	12 (48)	20 (48.8)	49 (72.1)	24 (72.7)	0.023

[a]Mean + SD.
[b]Median (range).
[c]Positive number (%).
*$P < 0.05$.

the other clinical groups. Similarly, patients with liver cirrhosis were significantly older when compared to asymptomatic carriers and patients with chronic hepatitis. Male predominance was observed in all groups with a maximum in the HCC group (81.8%) and minimum in the liver cirrhosis group (60.2%, $P = 0.041$). Ninety-seven (58.1%) patients infected with HCV were also positive for anti-HBc. The prevalence of anti-HBc was significantly higher in the HCC and liver cirrhosis groups with 72% when compared to chronic hepatitis 48.8% and asymptomatic carriers 58.1% ($P < 0.05$, Table I). Anti-HBs was detected in 19.8% (33/167) of patients infected with HCV with no significant difference found between the studied groups.

Detected HCV viremic cases tended toward a higher rate in the chronic hepatitis group 92.7% (38/41) compared to the asymptomatic carrier group (92.7% vs. 76%, $P = 0.072$), and a similar trend was observed in the HCVcAg level when the clinical groups were compared. To investigate the association between viral markers and progression of liver disease, 38 asymptomatic carrier and chronic hepatitis cases were compared to 38 age-sex-matched liver cirrhosis and patients with HCC (Table II). The prevalence of anti-HBc was the only significant difference between the two groups, with a higher rate in patients with progressive liver diseases ($P = 0.038$). HCV genotypes were determined in 65/76 of the age-sex-matched groups. Although no significant difference in the prevalence of HCV genotypes was found between the non-progressive and progressive liver disease groups, 4m and 4o were detected only in the latter group, and 1g prevalence was higher also in the latter, that is, patients with progressive liver disease.

Phylogenetic Analysis of the Core/E1 and NS5B Regions and Determination of the HCV Genotype/Subtype

Among the 167 anti-HCV-positive cases, HCV RNA positivity was examined by 5′UTR-targeted PCR (detection limit 1,000 copies/ml); in total 139 (83.2%) cases were positive and subjected to determination of HCV genotype by amplification, direct sequencing, and phylogenetic analysis based on the NS5B and/or the E1 regions. The HCV genotype was determined in a total of 129 (92.8%) of the 139 HCV RNA-positive cases. In 75/129 (58.1%), HCV phylogenetic analyses of the nucleotide sequences were available in both the core/E1 and NS5B regions simultaneously. In these 75 patients, no discrepancy was observed regarding the genotyping results as obtained by the phylogenetic analysis of both regions (E1 and NS5B), excluding possibility of presence of recombinant strains within these cases (Table III).

In the NS5B phylogeny, 89.7% (70/78) of samples were clustered with genotype 4 whereas 10.3% (10/78) were clustered with genotype 1g. Bootstrap values for all subtypes within genotype 4 was more than 75%, being lowest in the subtype 4a (BV = 79%). Eight samples were clustered with genotype 1g strains of Egyptian origin with BV of 100% (Fig. 2A). In the core/E1 phylogeny, BV was 99% for genotype 4a; 100% for genotypes 4n, 4l, 4o, and 4m; and 99% for genotype 1g (Fig. 2B). Inspection of the NS5B and core/E1 trees indicated no specific clustering by geographic regions in Egypt.

HCV Genotypes/Subtypes Among Different Governates in South Egypt

A total of 129 HCV samples which were genotyped were used to analyze the geographical distribution of HCV variants. Seventy-eight isolates belonged to the population studied in the Sohag governate, 39 isolates were from the Assuit governate population, and 12 isolates belonged to patients from the Qena governate. In south Egypt, the predominant genotype was HCV-4a (104/129, 80.6%), followed by genotype 1g (7.8%), genotype 4l (4.7%), then 4n (4.1%), and 4o (1.6%). Genotypes 4m and 4f were rarely found and were detected in 0.8% for each genotype. HCV genotype 4a was the predominant genotype in the Sohag governate and was detected in 88.5% (69/78) of the population studied, followed by genotype 1g (6.4%). Sporadic cases of infection with subtypes of genotype 4 (other than genotype 4a) were also observed including genotype 4o (2.6%), genotype 4f (1.3%), and genotype 4m (1.3%).

In the Assuit governate, HCV genotype 4a was observed in 64% (25/39), that is less frequently than in

TABLE II. Comparison Between Non-progressive and Progressive Liver Disease in Age and Gender-Matched Groups

	Total (n = 76)	Non-progressive liver disease (n = 38)	Progressive liver disease (n = 38)	*P*-value
Age[a]	45.6 ± 4.8	44.9 ± 5.4	46.3 ± 4.1	Matched
Gender (male)[b]	50 (65.8)	29 (76.3)	21 (55.3)	Matched
Asymptomatic carrier/chronic hepatitis/liver cirrhosis/HCC	6/32/30/8	6/32/0/0	0/0/30/8	
Anti-HBc[b]	40 (52.6)	15 (39.5)	25 (65.8)	0.038
Schistosoma Ab[b]	57 (80.3)	34 (89.5)	23/33 (70)	NS
HCV-RNA[b]	69 (90.8)	36 (94.7)	33 (86.8)	NS
HCV genotype[b]				
4a	50/65 (76.9)	26/35 (74.3)	24/30 (80)	NS
4n	4/65 (6.2)	4/35 (11.4)	0	NS
4l	4/65 (6.2)	4/35 (11.4)	0	NS
4m	1/65 (1.5)	0	1/30 (3.3)	NS
4o	2/65 (3.1)	0	2/30 (6.6)	NS
1g	4/65 (6.2)	1/35 (2.9)	3/30 (10)	NS

[a]Mean + SD.
[b]N (%).

TABLE III. Genotyping Results as Determined by Sequence and Phylogenetic Analysis of the E1 and NS5B Regions

	Classification based on NS5B								
Classification based on E1	1g	4a	4n	4l	4o	4m	4f	ND	Total
1g	8							2	10
4a		59						32	91
4n			2					2	4
4l				4				1	5
4o					1			1	2
4m						1			1
4f								1	1
ND		13	1	1					15
Total	8	72	3	5	1	1		39	129

the Sohag governate, genotype 1g found in 12.8%, genotype 4l in 10.3%, and genotype 4n in 12.8%. Only two genotypes were detected in patients from the Qena governate and they were genotype 4a (10/12, 83.3%) and genotype 4l (2/12, 16.7%) (Fig. 3). A significant difference in HCV genotypes distribution was observed between patients from the Sohag and Assuit governates, where incidence of infection with HCV genotype 4a was higher in the Sohag governate ($P = 0.002$). Infection with genotypes 4l and 4n was significantly higher in the population studied from the Assuit governate compared to the Sohag governate ($P = 0.003$, 0.011 respectively).

Clinical and Virological Characteristics of the Determinant HCV Genotypes/Subtypes

Clinical and virological characteristics were compared between patients infected with different variants of HCV; 104 cases infected with genotype 4a, 15 cases infected with genotype non-4a (including six cases with 4l, five cases with 4n, two cases with 4o, and one case with 4f, one with 4m), and 10 cases infected with HCV genotype 1g (Table IV). The mean age was similar between patients infected with different HCV genotypes. More patients among those infected with HCV-4a had liver cirrhosis than among patients infected with non-4a. More patients among those infected with (non-HCV-4a) had chronic hepatitis than among patients infected with HCV-4a. Interestingly, two cases were found to be infected with genotype 4o and both cases were patients with HCC. A significantly higher level of HCVcAg was observed in patients infected with HCV genotype 4a (median, range; 939.5, 24.7–13,219.2 fmol/L), compared to patients infected with genotype 1g strains (median, range; 203.1, 5.0–924.4 fmol/L) ($P < 0.0001$).

DISCUSSION

Genotype analysis of HCV within a defined population is an important issue in the study of the evolution of HCV infection in different geographical regions besides its importance for the development of an effective vaccine [Pybus et al., 2001; Cantaloube et al., 2005]. In addition, evidence supporting the differential pathogenicity of HCV subtypes has emerged in many studies. To the best of our knowledge, this is the first study concerned with the genetic diversity of HCV, and the clinical and virological characteristics of HCV infection in south Egypt.

Genotype 4 strains belonged to different subtypes including 4l, 4n, 4o, with solitary isolates of 4f and 4m together with the predominant genotype 4a in the population studied from south Egypt. Studies on the epidemic history of HCV in Egypt have indicated an exponential spread of the infection, occurring from the 1940s through 1980s; a period coinciding with mass campaigns of parenteral treatment for schistosomiasis [Tanaka et al., 2004, 2006]. This explosive epidemiological spread of HCV was also responsible for the simultaneous dissemination of multiple lineages of genotypes 4 and 1 [Pybus et al., 2003]. Genovese et al. [2005] indicated also the unexpected diversity of genotype 4 in a population studied in Alexandria in north-central Egypt compared to another study [Simmonds, 2004; Genovese et al., 2005]. However, the second most frequent subtype in the Alexendria study population was 4m (11% of cases), while that in the present study in patients from south Egypt was 4l (5% of HCV genotype 4), and genotype 4m was the less observed genotype in this cohort study. Genotype 1 was less frequent and only HCV genotype 1g was detected and observed in a considerable prevalence of the genotyped samples examined from this cohort. In a previous study where 68 blood donor specimens were selected from geographically distinct governates and analyzed phylogenetically genotype 1g was detected in 5/68 (7.4%), three of these five patients were from south Egypt [Ray et al., 2000].

The HCV prevalence throughout Egypt is associated directly with the amount of intravenous tartar emetic used to control schistosomiasis in the period, 1950–1980. The lowest rates were observed in Cairo and Alexendria (<8%), the highest in rural areas of the Nile Delta [Lower Egypt (>15%)], and intermediate prevalence (8–16%) in rural areas along the Nile south of Cairo (Middle and Upper Egypt) [Abdel-Aziz et al., 2000; Nafeh et al., 2000] which is the geographical area representing the samples collected in the current study. Geographical differences in the distribution of the HCV subtype was observed also between the Assuit and Sohag governates as represented by the presence of a high proportion of HCV subtypes 1g, 4l, and 4n in the former governates. The difference in the variability between the two governates might be explained by the fact that the Assuit governate, which is the largest town

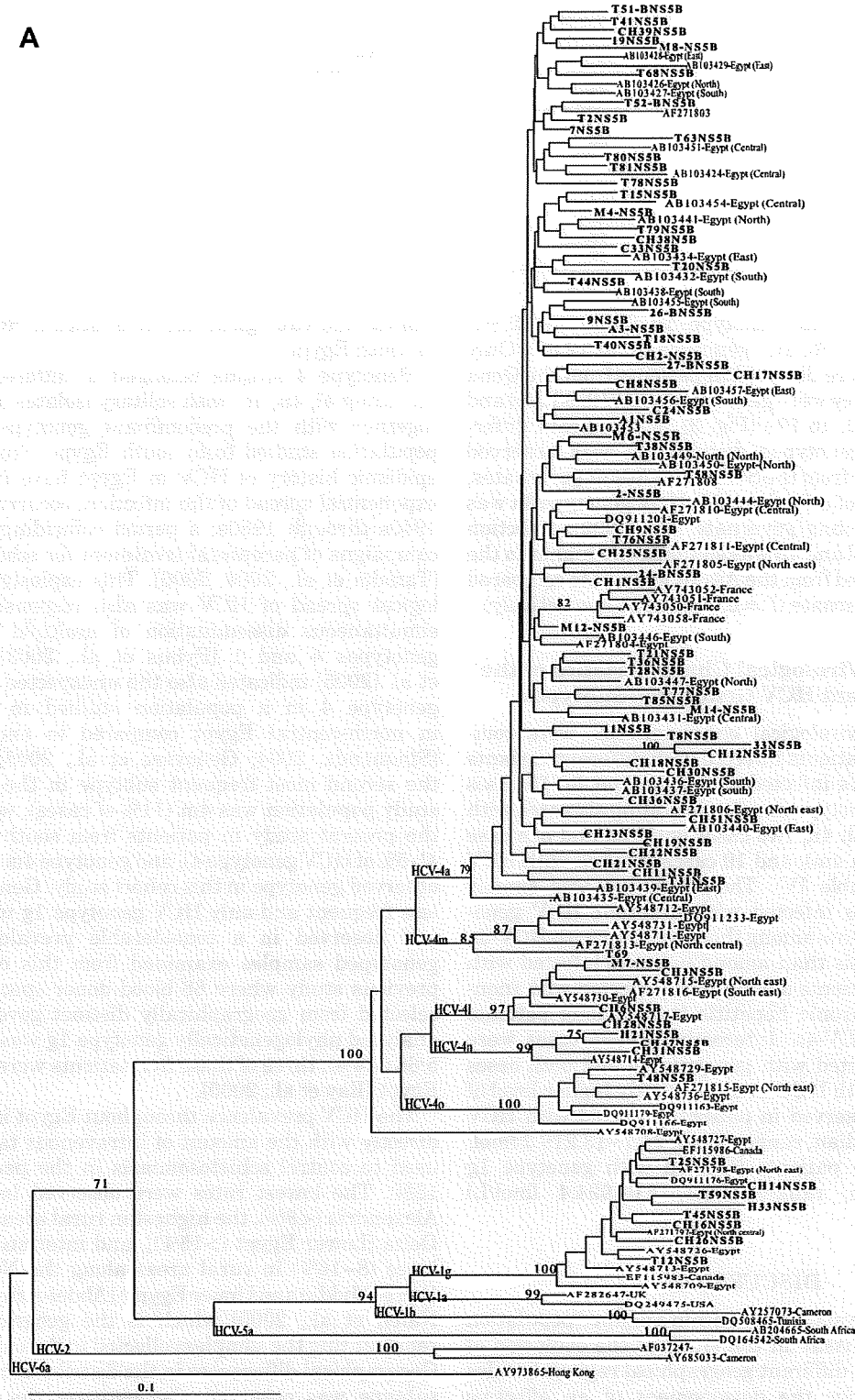

Fig. 2. Phylogenetic tree of the HCV (**A**) partial NS5B region sequences and (**B**) partial core/E1 region sequences isolated from patients infected with HCV in south Egypt (are indicated in bold) and a panel of reference strains retrieved from DDBJ/EMBL/GenBank identified by their accession number. The origins of reference strains are indicated. Data regarding the regional origin of HCV reference sequences of Egyptian origin are also indicated in parentheses when available in the GenBank database. Boot strap values are indicated in the tree root.

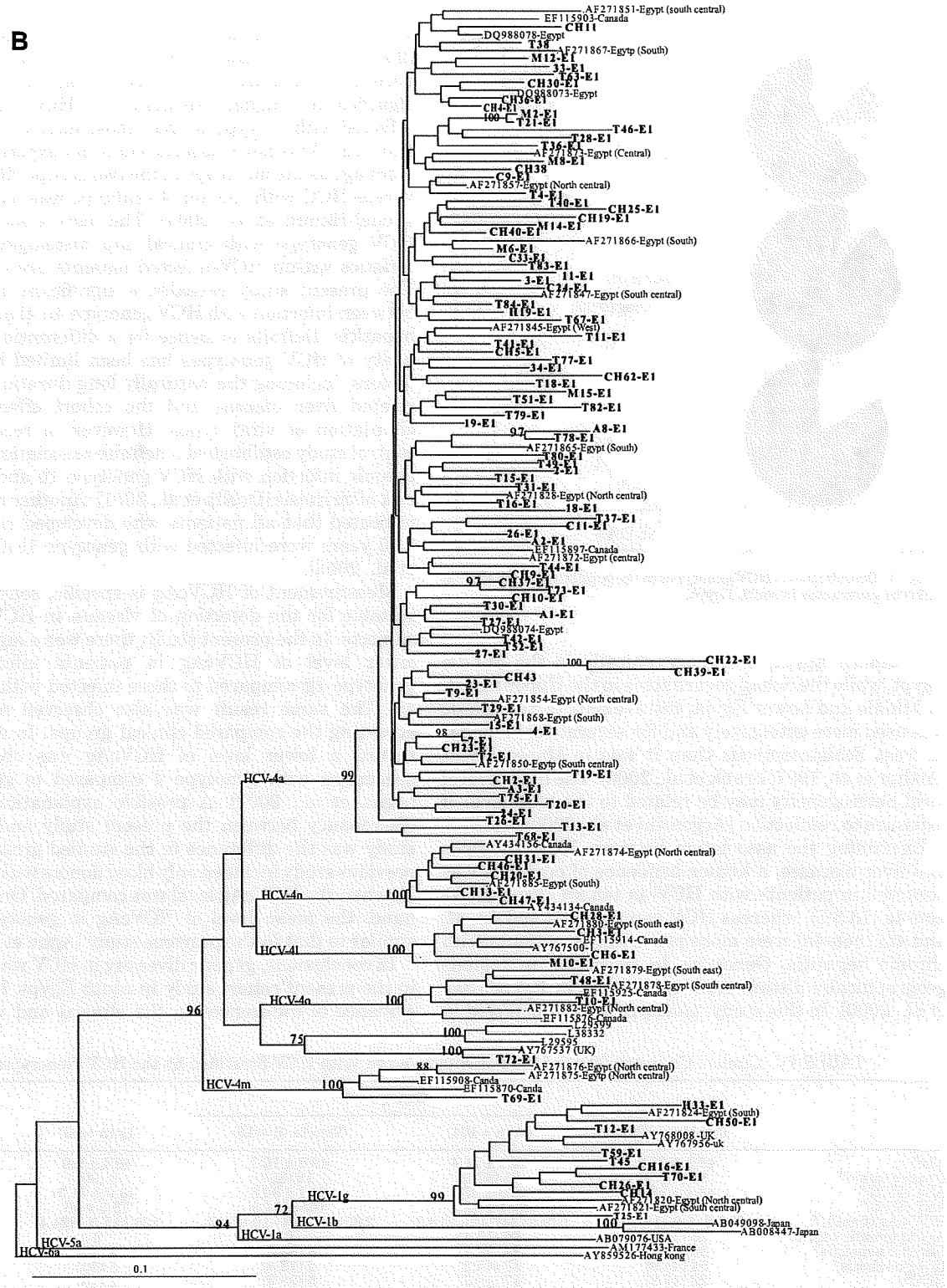

Fig. 2. (*Continued*)

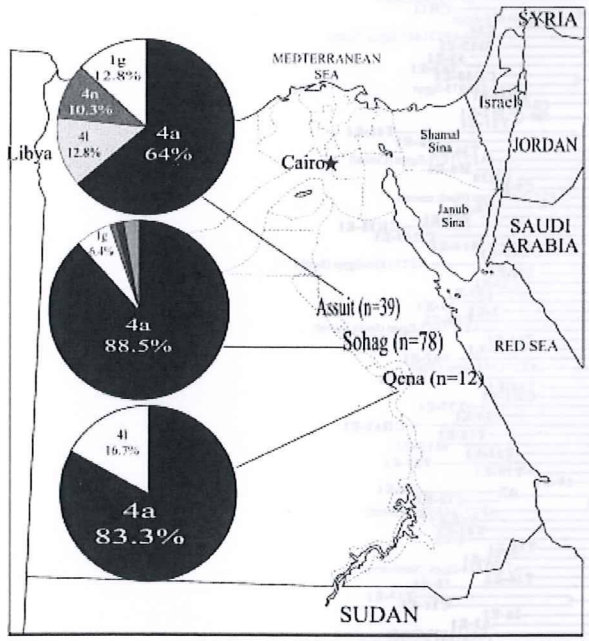

Fig. 3. Distribution of HCV genotypes in the population studied from different governates in south Egypt.

in southern Egypt, lies geographically in the Middle Egypt, while the Sohag governate is in the Upper Egypt. In Middle and Lower Egypt, intravenous tartar emetic was used more extensively and for several years longer to treat Schistosomiasis than it was in Upper Egypt [Arthur et al., 1997; Frank et al., 2000]. The high level of viral heterogeneity may be related to the high level of exposure to reinfection [Argentini et al., 2000].

Examining the association between HCV subtypes and liver diseases, a higher incidence of cirrhosis was observed in patients with HCV-4a (45.2%) than HCV-non-4a (13.3%), whereas HCV genotypes 4l and 4n, 4f, and 4m (non-4a) were more prevalent in patients with chronic hepatitis. Genotype 4o circulates in regions geographically distant from each other in Egypt [Ray et al., 2000]. In this study, genotype 4o was detected in 2/129 (1.6%). Interestingly both cases with genotype 4o were included in the HCC group. Abdel-Hamid et al. [2007] was the first to report the novel association between HCC and cluster subtype 4o as indicated by the significantly higher frequency of HCC in patients infected with subtype 4o than those infected with other subtypes. This novel association is not explained by the older age as the mean age in the two groups HCC with 4o versus HCC with the non-4o subtype was not different [Abdel-Hamid et al., 2007]. The data associating the HCV genotype with clinical and histological characteristics within HCV-infected patients are conflicting. The present study revealed a significant association between infection with HCV genotype 4n/4l and chronic hepatitis. Definite evidence for a differential pathogenicity of HCV genotypes has been limited by several factors, including the naturally long duration of HCV-related liver disease and the cohort effects in the circulation of viral types. However, a recent case–control study established a definite association between chronic infection with HCV genotype 1b and the high risk of cirrhosis [Osella et al., 2001]. Another report also indicated that all patients who developed cirrhosis in <10 years were infected with genotype 1b [Kurbanov et al., 2003].

Measurement of HCVcAg is specific, sensitive, and suitable for the detection of viremia in HCV-infected subjects. In the present study, there was a significantly lower level of HCVcAg in patients infected with genotype 1g compared to those infected with genotype 4a. The same result was also observed even after adjusting the compared clinical groups. In a previous report, a lower level of HCVcAg was observed in specimens with genotype 4 compared to genotype 1 [Agha et al., 2004]. A possible explanation for this discrepancy between the present study and previous study was the difference in the studied groups, as the previous study included only blood donors with genotype 1b when the HCVcAg level was compared. On the other hand, the mean level of HCVcAg in genotype 4 was similar to that in the previous study [Agha et al., 2004].

In conclusions, genetic diversity in HCV was detected in the present cohort study in south Egypt. Increasing evidence of differences in the clinical and virological

TABLE IV. Clinical Characteristics of the Patients Infected With HCV Stratified by the HCV Genotypes

		Genotype 4			
	Total (n = 129)	4a (n = 104)	Non-4a (n = 15)	1g (n = 10)	*P*-value
Age[a]	49.1 ± 11.2	49.1 ± 11.4	49.2 ± 10.7	48.4 ± 9.9	NS
Gender (male)[b]	91 (70.5)	70 (67.3)	12 (80)	9 (90)	NS
ALT (IU/L)[a]	43.4 ± 28.9	40.8 ± 27.8	60.1 ± 30.8	43.0 ± 31.0	0.049[d]
AST (IU/L)[a]	68.5 ± 48.3	62.1 ± 43.3	105 ± 64.3	73.6 ± 46	0.035[d]
HCV-cAg (fmol/L)[c]	897.2 (5.0–19,654)	939.5 (24.7–13,219.2)	2,354.8 (59.4–19,654.2)	203.1 (5.0–924.4)	<0.0001[e]
Asymptomatic carrier[b]	16 (12.4)	16 (15.4)	0	0	NS
Chronic hepatitis[b]	36 (27.9)	24 (23.1)	8 (53.3)	4 (40)	0.025[d]
Liver cirrhosis[b]	54 (41.9)	47 (45.2)	2 (13.3)	5 (50)	0.023[d]
HCC[b]	23 (17.8)	17 (16.3)	5 (33.3)	1 (10)	NS

[a]Mean + SD.
[b]N (%).
[c]Median (range).
[d]Patients infected with HCV genotype 4a versus patients infected with HCV-4 non-subtype 4a.
[e]Patients infected with HCV genotype 4a versus patients infected with 1g.

characteristics of the isolated strains between different genotypes/subtypes has been introduced in the present study. The data highlight the need for further studies exploring the HCC mortality burden within different districts in Egypt; a country with the highest HCV prevalence in the world. There is also a need for a case–control study to investigate the trends in the association of HCC development with infection by HCV genotype 4o.

REFERENCES

Abdel-Aziz F, Habib M, Mohamed MK, Abdel-Hamid M, Gamil F, Madkour S, Mikhail NN, Thomas D, Fix AD, Strickland GT, Anwar W, Sallam I. 2000. Hepatitis C virus (HCV) infection in a community in the Nile Delta: Population description and HCV prevalence. Hepatology 32:111–115.

Abdel-Hamid M, El-Daly M, Molnegren V, El-Kafrawy S, Abdel-Latif S, Esmat G, Strickland GT, Loffredo C, Albert J, Widell A. 2007. Genetic diversity in hepatitis C virus in Egypt and possible association with hepatocellular carcinoma. J Gen Virol 88:1526–1531.

Abdel-Wahab MF, Zakaria S, Kamel M, Abdel-Khaliq MK, Mabrouk MA, Salama H, Esmat G, Thomas DL, Strickland GT. 1994. High seroprevalence of hepatitis C infection among risk groups in Egypt. Am J Trop Med Hyg 51:563–567.

Agha S, Tanaka Y, Saudy N, Kurbanov F, Abo-Zeid M, El-Malky M, Khalaf M, Ohta N, Yoshizawa H, Mizokami M. 2004. Reliability of hepatitis C virus core antigen assay for detection of viremia in HCV genotypes 1, 2, 3, and 4 infected blood donors: A collaborative study between Japan, Egypt, and Uzbekistan. J Med Virol 73:216–222.

Aoyagi K, Ohue C, Iida K, Kimura T, Tanaka E, Kiyosawa K, Yagi S. 1999. Development of a simple and highly sensitive enzyme immunoassay for hepatitis C virus core antigen. J Clin Microbiol 37:1802–1808.

Argentini C, Dettori S, Villano U, Guadagnino V, Infantolino D, Dentico P, Coppola RC, Rapicetta M. 2000. Molecular characterisation of HCV genotype 4 isolates circulating in Italy. J Med Virol 62:84–90.

Arthur RR, Hassan NF, Abdallah MY, el-Sharkawy MS, Saad MD, Hackbart BG, Imam IZ. 1997. Hepatitis C antibody prevalence in blood donors in different governorates in Egypt. Trans R Soc Trop Med Hyg 91:271–274.

Cantaloube JF, Gallian P, Attoui H, Biagini P, De Micco P, de Lamballerie X. 2005. Genotype distribution and molecular epidemiology of hepatitis C virus in blood donors from southeast France. J Clin Microbiol 43:3624–3629.

Choo QL, Richman KH, Han JH, Berger K, Lee C, Dong C, Gallegos C, Coit D, Medina-Selby R, Barr PJ, Weiner AJ, Bradley DW, Kuo G, Houghton M. 1991. Genetic organization and diversity of the hepatitis C virus. Proc Natl Acad Sci USA 88:2451–2455.

Dhaliwal SK, Prescott LE, Dow BC, Davidson F, Brown H, Yap PL, Follett EA, Simmonds P. 1996. Influence of viraemia and genotype upon serological reactivity in screening assays for antibody to hepatitis C virus. J Med Virol 48:184–190.

Frank C, Mohamed MK, Strickland GT, Lavanchy D, Arthur RR, Magder LS, El Khoby T, Abdel-Wahab Y, Aly Ohn ES, Anwar W, Sallam I. 2000. The role of parenteral antischistosomal therapy in the spread of hepatitis C virus in Egypt. Lancet 355:887–891.

Genovese D, Dettori S, Argentini C, Villano U, Chionne P, Angelico M, Rapicetta M. 2005. Molecular epidemiology of hepatitis C virus genotype 4 isolates in Egypt and analysis of the variability of envelope proteins E1 and E2 in patients with chronic hepatitis. J Clin Microbiol 43:1902–1909.

Hnatyszyn HJ. 2005. Chronic hepatitis C and genotyping: The clinical significance of determining HCV genotypes. Antivir Ther 10:1–11.

Kurbanov F, Tanaka Y, Sugauchi F, Kato H, Ruzibakiev R, Zalyalieva M, Yunusova Z, Mizokami M. 2003. Hepatitis C virus molecular epidemiology in Uzbekistan. J Med Virol 69:367–375.

Nafeh MA, Medhat A, Shehata M, Mikhail NN, Swifee Y, Abdel-Hamid M, Watts S, Fix AD, Strickland GT, Anwar W, Sallam I. 2000. Hepatitis C in a community in Upper Egypt: I. Cross-sectional survey. Am J Trop Med Hyg 63:236–241.

Ohno O, Mizokami M, Wu RR, Saleh MG, Ohba K, Orito E, Mukaide M, Williams R, Lau JY. 1997. New hepatitis C virus (HCV) genotyping system that allows for identification of HCV genotypes 1a, 1b, 2a, 2b, 3a, 3b, 4, 5a, and 6a. J Clin Microbiol 35:201–207.

Osella AR, Misciagna G, Guerra V, Elba S, Buongiorno G, Cavallini A, Di Leo A, Sonzogni L, Mondelli MU, Silini EM. 2001. Hepatitis C virus genotypes and risk of cirrhosis in southern Italy. Clin Infect Dis 33:70–75.

Purcell R. 1997. The hepatitis C virus: Overview. Hepatology 26:11S–14S.

Pybus OG, Charleston MA, Gupta S, Rambaut A, Holmes EC, Harvey PH. 2001. The epidemic behavior of the hepatitis C virus. Science 292:2323–2325.

Pybus OG, Drummond AJ, Nakano T, Robertson BH, Rambaut A. 2003. The epidemiology and iatrogenic transmission of hepatitis C virus in Egypt: A Bayesian coalescent approach. Mol Biol Evol 20:381–387.

Ray SC, Arthur RR, Carella A, Bukh J, Thomas DL. 2000. Genetic epidemiology of hepatitis C virus throughout Egypt. J Infect Dis 182:698–707.

Saito I, Miyamura T, Ohbayashi A, Harada H, Katayama T, Kikuchi S, Watanabe Y, Koi S, Onji M, Ohta Y, Choo QL, Houghton M, Kuo G. 1990. Hepatitis C virus infection is associated with the development of hepatocellular carcinoma. Proc Natl Acad Sci USA 87:6547–6549.

Shin-I T, Tanaka Y, Tateno Y, Mizokami M. 2008. Development and public release of a comprehensive hepatitis virus database. Hepatol Res 38:234–243.

Simmonds P. 2004. Genetic diversity and evolution of hepatitis C virus—15 years on. J Gen Virol 85:3173–3188.

Simmonds P, Holmes EC, Cha TA, Chan SW, McOmish F, Irvine B, Beall E, Yap PL, Kolberg J, Urdea MS. 1993. Classification of hepatitis C virus into six major genotypes and a series of subtypes by phylogenetic analysis of the NS-5 region. J Gen Virol 74:2391–2399.

Simmonds P, Bukh J, Combet C, Deleage G, Enomoto N, Feinstone S, Halfon P, Inchauspe G, Kuiken C, Maertens G, Mizokami M, Murphy DG, Okamoto H, Pawlotsky JM, Penin F, Sablon E, Shin IT, Stuyver LJ, Thiel HJ, Viazov S, Weiner AJ, Widell A. 2005. Consensus proposals for a unified system of nomenclature of hepatitis C virus genotypes. Hepatology 42:962–973.

Smith DB, Pathirana S, Davidson F, Lawlor E, Power J, Yap PL, Simmonds P. 1997. The origin of hepatitis C virus genotypes. J Gen Virol 78:321–328.

Takeuchi T, Katsume A, Tanaka T, Abe A, Inoue K, Tsukiyama-Kohara K, Kawaguchi R, Tanaka S, Kohara M. 1999. Real-time detection system for quantification of hepatitis C virus genome. Gastroenterology 116:636–642.

Tanaka Y, Hanada K, Mizokami M, Yeo AE, Shih JW, Gojobori T, Alter HJ. 2002. Inaugural Article: A comparison of the molecular clock of hepatitis C virus in the United States and Japan predicts that hepatocellular carcinoma incidence in the United States will increase over the next two decades. Proc Natl Acad Sci USA 99:15584–15589.

Tanaka Y, Agha S, Saudy N, Kurbanov F, Orito E, Kato T, Abo-Zeid M, Khalaf M, Miyakawa Y, Mizokami M. 2004. Exponential spread of hepatitis C virus genotype 4a in Egypt. J Mol Evol 58:191–195.

Tanaka Y, Kurbanov F, Mano S, Orito E, Vargas V, Esteban JI, Yuen MF, Lai CL, Kramvis A, Kew MC, Smuts HE, Netesov SV, Alter HJ, Mizokami M. 2006. Molecular tracing of the global hepatitis C virus epidemic predicts regional patterns of hepatocellular carcinoma mortality. Gastroenterology 130:703–714.

Thompson JD, Higgins DG, Gibson TJ. 1994. CLUSTAL W: Improving the sensitivity of progressive multiple sequence alignment through sequence weighting, position-specific gap penalties and weight matrix choice. Nucleic Acids Res 22:4673–4680.

WHO. 1999. Global surveillance and control of hepatitis C. Report of a WHO Consultation organized in collaboration with the Viral Hepatitis Prevention Board, Antwerp, Belgium. J Viral Hepat 6:35–47.

Zein NN. 2000. Clinical significance of hepatitis C virus genotypes. Clin Microbiol Rev 13:223–235.

RESEARCH COMMUNICATION

Essential role of Tip60-dependent recruitment of ribonucleotide reductase at DNA damage sites in DNA repair during G1 phase

Hiroyuki Niida,[1] Yuko Katsuno,[1] Misuzu Sengoku,[1] Midori Shimada,[1] Megumi Yukawa,[1] Masae Ikura,[2] Tsuyoshi Ikura,[2] Kazuteru Kohno,[3] Hiroki Shima,[3] Hidekazu Suzuki,[3] Satoshi Tashiro,[3] and Makoto Nakanishi[1,4]

[1]Department of Cell Biology, Graduate School of Medical Sciences, Nagoya City University Medical School, Nagoya 467-8601, Japan; [2]Radiation Biology Center, Kyoto University, Kyoto 606-8501, Japan; [3]Department of Cell Biology, Research Institute for Radiation Biology and Medicine (RIRBM), Hiroshima University, Hiroshima 734-8553, Japan

A balanced deoxyribonucleotide (dNTP) supply is essential for DNA repair. Here, we found that ribonucleotide reductase (RNR) subunits RRM1 and RRM2 accumulated very rapidly at damage sites. RRM1 bound physically to Tip60. Chromatin immunoprecipitation analyses of cells with an I-SceI cassette revealed that RRM1 bound to a damage site in a Tip60-dependent manner. Active RRM1 mutants lacking Tip60 binding failed to rescue an impaired DNA repair in RRM1-depleted G1-phase cells. Inhibition of RNR recruitment by an RRM1 C-terminal fragment sensitized cells to DNA damage. We propose that Tip60-dependent recruitment of RNR plays an essential role in dNTP supply for DNA repair.

Supplemental material is available at http://www.genesdev.org.

Received September 15, 2009; revised version accepted December 22, 2009.

Maintenance of the optimal intracellular concentrations of deoxyribonucleotides (dNTPs) is critical not only for faithful DNA synthesis during DNA replication and repair, but also for the survival of all organisms. Ribonucleotide reductase (RNR), composed of a tetrameric complex of two large catalytic (RRM1) subunits and two small subunits (RRM2 or 53R2), catalyzes de novo synthesis of dNTPs from the corresponding ribonucleotides (Reichard 1993). This reaction is the rate-limiting process in DNA precursor synthesis and is regulated by multiple complex mechanisms, including transcriptional and subcellular localization regulation of RNR (Nordlund and Reichard 2006). In order to duplicate their chromosomal DNA, mammalian S-phase cells possess 15–20 times more dNTP pools than resting quiescent cells, whereas whole dNTP pools were almost unchanged after DNA damage, suggesting the presence of a unique mechanism that supplies a sufficient quantity of dNTPs at repair sites (Hakansson et al. 2006). DNA synthesis must function properly in both repair and replication (dNTP concentrations in fibroblasts were estimated to be as follows: ~0.5 μM in G0/G1-phase cells, and ~10 μM in S-phase cells, given that the average volume of a fibroblast is 3.4 pL) (Imaizumi et al. 1996). Although the amount of dNTPs required for DNA repair is small, their concentration during DNA synthesis is critical because DNA polymerase involved in DNA repair (Kraynov et al. 2000; Johnson et al. 2003) has similar kinetic affinities for dNTPs (~10 μM) to those involved in DNA replication (~10 μM) (Dong and Wang 1995). Therefore, the dNTPs might be compartmentalized close to the damage sites during the DNA repair process. In this study, we show that, in mammals, both RRM1 and RRM2 rapidly accumulated at double-strand break (DSB) sites in a Tip60-binding-dependent manner.

[*Keywords*: DNA repair; ribonucleotide reductase; Tip60; dNTPs; genomic instability; DNA double-strand breaks]

[4]Corresponding author.
E-MAIL mkt-naka@med.nagoya-cu.ac.jp, FAX 81-52-842-3955.

Article is online at http://www.genesdev.org/cgi/doi/10.1101/gad.1863810.

Results and Discussion

In order to understand the mechanisms by which dNTPs are sufficiently supplied at DNA damage sites in mammals, we first examined changes in the subcellular localization of RRM1 and RRM2 subunits after ionizing irradiation (IR) irradiation. Although both RRM1 and RRM2 predominantly localized in the cytoplasm as reported previously (Pontarin et al. 2008), we also detected trace, but significant, signals of both proteins in chromatin fraction (see Fig. 1C; Supplemental Fig. S4A–D). After removing soluble RNR proteins by detergent extraction, we found that RRM1 and RRM2 proteins formed nuclear foci that colocalized with γH2AX (Fig. 1A). RRM1 nuclear foci were not evident without DNA damage (Supplemental Fig. S1A) or after RRM1 depletion by siRNA (Supplemental Fig. S1B). Ultravioulet A (UVA) microirradiation resulted in the accumulation of RRM1 and RRM2 along microirradiated lines as early as 5 min after treatment (Fig. 1B). These accumulations were also observed when cells were not subjected to detergent extraction or preincubation with BrdU (Supplemental Fig. S2A,B), but were significantly compromised when R1 expression was knockdown by siRNA (Supplemental Figs. S2C, S4B), excluding the possibility that accumulated signals at DSB sites were artifacts during cell-staining processes. These results indicated that RNR, at least in part, was rapidly recruited to DSB sites.

In order to determine the molecular basis underlying RNR recruitment at the sites of DSBs, we performed yeast two-hybrid screening using RRM1 as a bait. Of a total of 5×10^6 transformants from a HeLa cell cDNA library, 45 positive colonies were confirmed to be lacZ-positive. They contained overlapping cDNAs derived from three genes: *RRM2* and *53R2* (both encoding a small subunit of RNR), and another encoding *Tip60* histone acetyltransferase (Tip60). Small C-terminal RRM1 deletion mutants (Δ761-C and Δ781-C) failed to bind Tip60, but retained the ability to bind to RRM2 (Supplemental Fig. S3A). In contrast, the N-terminal truncation mutant of Tip60

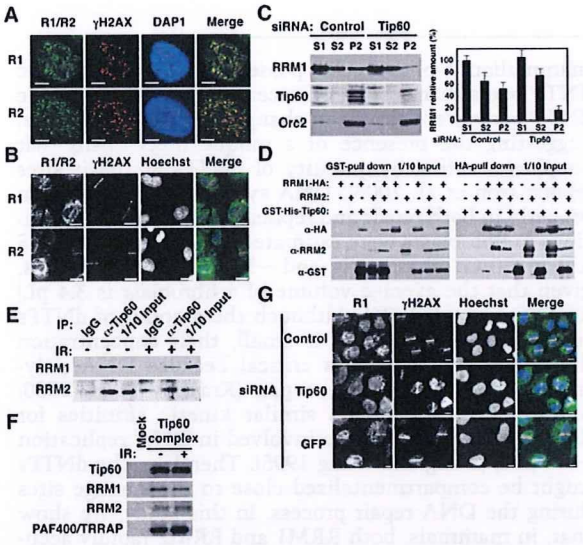

Figure 1. Tip60-dependent recruitment of RNR at DSB sites. (*A*) HeLa cells were exposed to IR at 1 Gy, subjected to in situ detergent extraction after 5 min, and immunostained with the indicated antibodies. Bars, 5 μm. (*B*) GM02063 cells were subjected to UVA microirradiation and immunostained with the indicated antibodies after 5 min. RRM1 or RRM2 and γH2AX signals are shown in green and red, respectively, in merged images. Bars, 10 μm. (*C*) IR-irradiated HeLa cell lysates treated with the indicated siRNAs were fractionated as described in the Materials and Methods. (*Left* panels) The fractions were subjected to immunoblotting using the indicated antibodies. (*Right* panel) The RRM1 bands were quantitated, and the results are presented as percentages of S1 fraction. Data are mean ± standard deviation (n = 3). (*D*) Sf9 lysates expressing RRM1-HA, RRM2, or GST-His-Tip60 were subjected to GST pull-down or HA pull-down assays using the indicated antibodies. (*E*) Chromatin fractions from IR- or mock-treated HeLa cells (after 5 min) were solubilized with micrococcal nuclease. The solubilized extracts were immunoprecipitated with anti-Tip60 antibodies or control IgG. The resulting precipitates and a 10% input (1/10 Input) were immunoblotted with the indicated antibodies. (*F*) The affinity-purified Tip60 complexes, as described in the Materials and Methods, were subjected to immunoblotting using the indicated antibodies. (*G*) GM02063 cells were treated with control, Tip60, or GFP siRNAs and then subjected to UVA microirradiation as in *B*.

(TC2) could interact with RRM1, but no mutant with any additional truncation of TC2 was able to do so (Supplemental Fig. S3B). Full-length Tip60 failed to bind full-length RRM2 (Supplemental Fig. S3C). We generated the C-terminal fragment of RRM1 (amino acids 701–792) with a SV40 nuclear localization signal (NLS-RC1-HA) and examined its ability to bind Tip60 in vivo and in vitro. NLS-RC1-HA, but not a control NL-GFP-HA fragment, was detected in the anti-Myc immunoprecipitates when transiently coexpressed with Tip60-Myc (Supplemental Fig. S3D). Purified MBP-fused RC1 produced in *Escherichia coli* was capable of binding to GST-Tip60 expressed in insect cells (Supplemental Fig. S3E). Both Δ761-C and Δ781-C failed to bind chromatin, further confirming that the binding of RRM1 to chromatin required its interaction with Tip60 (Supplemental Fig. S3F).

Similarly to Chk1 (Niida et al. 2007; Shimada et al. 2008), endogenous RRM1 was present in cytosolic (S1), nucleoplasmic (S2), and chromatin-bound (P2) fractions (Supplemental Fig. S4A). Tip60 existed predominantly in the chromatin-bound fraction (P2). Both RRM1 and Tip60 proteins in this fraction were partly solubilized by treatment with micrococcal nuclease (Mnase), suggesting that they associated with chromatin. RRM1 knockdown showed a significant decrease of RRM1 protein levels in both soluble and chromatin-bound fractions (Supplemental Fig. S4B). IKKα and Orc2 were detected predominantly in soluble and chromatin fractions, respectively, indicating that cell fractionation was done successfully. Ectopic RRM1-HA present in the chromatin fraction was increased when Tip60-Myc-His was coexpressed, although a low level of RRM1-HA was detected in the absence of Tip60-Myc-His, presumably due to the presence of endogenous Tip60 (Supplemental Fig. S4C). The amounts of RRM1 and Tip60 bound to the chromatin were not affected by DNA damage (Supplemental Fig. S4D). However, depletion of Tip60 resulted in a reduction in the amount of RRM1 on chromatin (Fig. 1C). Taken together, chromatin binding of RRM1 appeared to be Tip60-dependent. RRM1-HA, but not the RRM2 subunit alone, formed a complex with GST-His-Tip60 in insect cells (Fig. 1D, left panels). RRM2 also formed a complex with GST-His-Tip60 in a manner dependent on the presence of RRM1-HA. Consistently, accumulation of RRM2 at DSB sites was compromised when RRM1 was depleted (Supplemental Fig. S2D). Immunoprecipitations using anti-HA antibodies demonstrated that RRM1-HA bound to both RRM2 and GST-His-Tip60 (Fig. 1D, right panels). RRM1 and RRM2 were detected in the precipitates of anti-Tip60 antibodies from the solubilized chromatin, even in the absence of DNA damage (Fig. 1E). To further confirm the interaction between RNR and Tip60, we purified the Tip60 complex from HeLa cell nuclear extracts expressing Flag-HA Tip60 as reported previously (Ikura et al. 2000, 2007). RRM1 and RRM2, as well as PAF400/TRRAP as a positive control (Murr et al. 2006), were detected in Tip60 complex from extracts with or without DNA damage (Fig. 1F). Tip60 knockdown by siRNA or shRNA abrogated accumulation of RRM1 along with microirradiated lines (Fig. 1G; Supplemental Fig. S2E). These results suggested that RRM1 recruitment at DSB sites was Tip60-dependent.

To determine precisely whether RRM1 was recruited at the site of DNA damage, we generated *Ku*-deficient mouse embryonic fibroblasts (MEFs) in which a single DSB was introduced after infection with adenoviruses expressing I-SceI. This DSB was not rapidly repaired by nonhomologous end-joining, making it easy to detect proteins accumulating at this DSB site by chromatin immunoprecipitation (ChIP) analysis (*STEFKu70*$^{-/-}$*phprt-DR-GFP*) (Fig. 2A; Pierce et al. 2001). Introduction of the DSB was confirmed by Southern blotting (Supplemental Fig. S5). ChIP analyses revealed a substantial increase in the binding of RRM1 as well as Rad51 and Tip60 to a DNA break site. An increase in acetylation of histone H4 was also observed at the damage site (Fig. 2B). These were not seen on infection with control LacZ. Tip60 depletion by two independent siRNAs resulted in a loss of RRM1 binding to a DSB site, as well as a reduction in acetylation of histone H4 (Fig. 2C). A mutant Tip60 lacking histone-acetylating activity could recruit RRM1 to the DSB site similarly to wild-type RRM1 (Supplemental Fig. S6A). Inhibition of ATM, ATR, and DNA-PK by caffeine did not affect RRM1 recruitment (Supplemental Fig. S6B). These results further supported the notion that complex

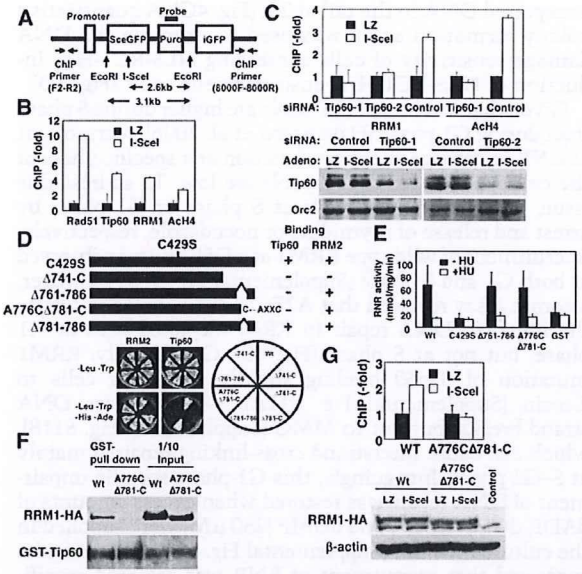

Figure 2. RRM1 is recruited at DSB sites in a Tip60-dependent manner. (*A*) Map of the I-SceI cassette construct containing the I-SceI site, the probe for Southern blotting, and a set of primers for the ChIP assay. (*B*) *STEFKu70*$^{-/-}$*phprt-DR-GFP* cells infected with I-SceI adenoviruses were subjected to ChIP analysis using the indicated antibodies as described in the supporting Materials and Methods. Data are shown as percentages of increases in PCR products from cells expressing I-SceI (I-SceI) relative to those from cells expressing Lac Z (LZ). Data are mean ± standard deviation (n = 3). (*C*) *STEFKu70*$^{-/-}$*phprt-DR-GFP* cells were transfected with two independent Tip60 siRNAs (Tip60-1 and Tip60-2) or control siRNA. ChIP analysis was performed as in *B*. (*Bottom* panels) Aliquots of cell lysates were subjected to immunoblotting using anti-Tip60 antibodies. (*D*) The constructs used are schematically represented, and the specific interaction between RRM1 mutants and Tip60 was assayed using yeast two-hybrid screening. (*E*) An in vitro RNR assay of complexes containing wild-type or various RRM1 mutants was performed as described in the Materials and Methods. (Black bars) −HU; (white bars) +HU (10 mM). Data are mean ± standard deviation (n = 3). (*F*) Sf9 lysates expressing GST-His-Tip60 and the indicated RRM1-HA were subjected to GST pull-down assay using the indicated antibodies. (*G*) Knockout–knock-in *STEFKu70*$^{-/-}$*phprt-DR-GFP* cells expressing wild-type or A776CΔ781-C RRM1-HA were generated by transfection with vectors for either wild-type or A776CΔ781-C RRM1 and then with RRM1 siRNA. Expression vectors of wild type and A776CΔ781-C contain mutations in a specific sequence targeted by siRNA. (*Top* panel) Cells were subjected to ChIP analysis using anti-HA antibodies as in *B*. (*Bottom* panels) Aliquots of cell lysates were subjected to immunoblotting using the indicated antibodies.

formation between RNR and Tip60 is required for recruitment of RNR to sites of DNA damage.

We then examined if RNR recruitment at damage sites was required for effective DNA repair. We first generated RRM1 mutants that lack the ability to bind Tip60 but retain RNR activity. Given that the C-terminal CXXC motif of RRM1 is important for RNR function (Zhang et al. 2007), we constructed *RRM1* mutants containing the CXXC motif but lacking Tip60-binding ability (Δ761–786 and A776CΔ781-C) (Fig. 2D). Wild-type RRM1 or its mutants were coexpressed with RRM2 in insect cells, and the resultant complexes were subjected to an in vitro RNR assay (Fukushima et al. 2001). RNR complexes containing wild-type, Δ761–786, and A776CΔ781-C RRM1 retained hydroxyurea (HU)-sensitive RNR activity (HU is a specific RNR inhibitor), whereas an inactive C429S mutant or GST protein as a negative control did not show RNR activity (Fig. 2E). The specific activity of RNR containing wild-type, Δ761–787, and A776CΔ781-C RRM1 (~50 nmol/mg per minute) was similar to that reported previously (Guittet et al. 2001), confirming the reliability of our results. The A776CΔ781-C mutant failed to form a complex with GST-Tip60 (Fig. 2F). ChIP analysis using RRM1 knockout–knock-in *STEFKu70*$^{-/-}$*phprt-DR-GFP* cells revealed that the A776CΔ781-C mutant failed to accumulate at the DSB site (Fig. 2G). These results indicated that direct interaction of RRM1 to Tip60 is required for triggering its accumulation at the DSB site.

A comet assay revealed that DNA damage in cells was repaired efficiently within 1 h in the absence of HU. However, treatment with HU, and RRM1 or RRM2 depletion, resulted in an impairment of DNA repair (Fig. 3A,B). RNR activity was thus essential for effective repair. Ectopic expression of wild-type *RRM1* with mutations in a specific sequence targeted by siRNA effectively rescued the impaired DNA repair in cells depleted of endogenous RRM1 (Fig. 3C). In contrast, ectopic expression of C429S, Δ761–786, and A776CΔ781-C RRM1 failed

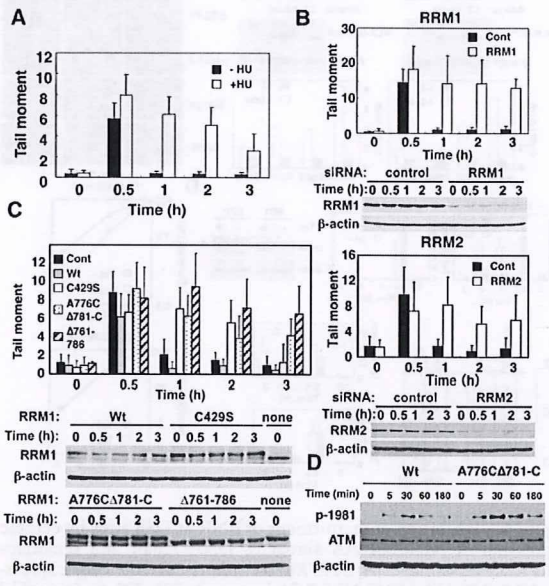

Figure 3. Recruitment of active RNR at DNA damage sites is a prerequisite for effective DNA repair. (*A*) HeLa cells were treated with (open bars) or without (filled bars) 2.5 mM HU, exposed to IR (4 Gy), and subjected to a comet assay as described in the Materials and Methods. The results were obtained by counting at least 50 cells per sample in three independent experiments. (*B*) HeLa cells were transfected with a control (filled bars) or RRM1 or RRM2 siRNA (open bars), and DNA repair was evaluated as in *A*. Cell lysates were subjected to immunoblotting using the indicated antibodies. (*C*) HeLa cells were transfected with or without (filled bars) either wild-type (gray bars), C429S (open bars), A776CΔ781-C (dotted), or Δ761–786 (hatched) RRM1. RRM1-transfected cells were then transfected with RRM1 siRNA. Expression vectors of wild type and various RRM1 mutants contain mutations in a specific sequence targeted by siRNA. DNA repair activity and expression of RRM1 were examined as in *B*. (*D*) Knockout–knock-in HeLa cells expressing wild type or A776CΔ781-C RRM1-HA were exposed to IR, and cell lysates were subjected to immunoblotting as in *C*.

to do so. ATM was activated independently of Tip60 binding to RNR, but this activation was enhanced and prolonged in cells expressing A776CΔ781-C, presumably due to impaired DNA repair (Fig. 3D). It is therefore conceivable that recruitment of active RNR at DNA damage sites is a prerequisite for effective DSB repair, but not for activation of checkpoint signaling. Tip60 is also known to participate in transcriptional regulation of several genes. Neither RRM1 nor RRM2 proteins were affected by Tip60 depletion or overexpression (Supplemental Fig. S7), indicating that the effect of Tip60 did not result from changes in RRM1 and RRM2 expression.

ChIP analyses revealed that NLS-RC1-HA specifically inhibited RRM1 binding, but did not affect Rad51 or Tip60 binding, or increase H4 acetylation at the DSB site in *STEFKu70*$^{-/-}$*phprt-DR-GFP* cells (Fig. 4A). Expression of NLS-RC1-HA suppressed accumulation of endogenous RRM1 at DNA damage sites (Supplemental Fig. S8A,B), but did not affect the foci formation of 53BP1 at DSB sites (Fig. 4B), or complex formation and activity (Supplemental Fig. S9A,B) of endogenous RNR. However, cells expressing NLS-RC1-HA, but not NLS-GFP-HA, had unrepaired DNA in the tail at 2 h (Fig. 4C). A quantitative colony formation assay was used to examine the DNA damage sensitivity of cells expressing NLS-RC1-HA. Induction of NLS-RC1-HA sensitized cells to IR (Fig. 4D).

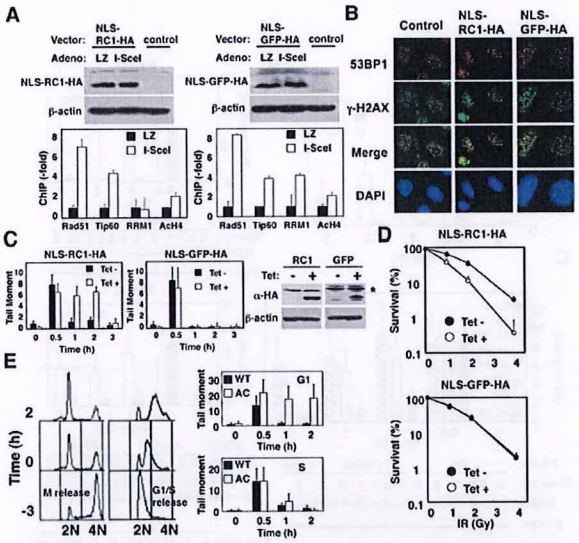

Figure 4. Inhibition of recruitment of RNR at DSB sites by ectopic expression of NLS-RC1-HA abrogates DNA repair and sensitizes cells to DNA damage. (*A*) *STEFKu70*$^{-/-}$*phprt-DR-GFP* cells expressing NLS-RC1-HA (SV40 NLS-RC1 fragment, 701–792 amino acids) or NLS-GFP-HA (GFP fragment, 1–93 amino acids) were subjected to ChIP analysis as in Figure 2B. (*Top* panels) Cell lysates were subjected to immunoblotting using the indicated antibodies. (*B*, *left* panels) Tet-on HeLa cells expressing NLS-RC1-HA or NLS-GFP-HA were treated with or without tetracycline (1 μg/mL), exposed to IR (4 Gy), and subjected to immunostaining with the indicated antibodies and a comet assay as in Figure 3A. (*Right* panels) IR-untreated lysates were subjected to immunoblotting using the indicated antibodies. (*C*) Asterisk (*) represents nonspecific bands. (*D*) These cells were exposed to the indicated dose of IR, and a quantitative colony formation assay was performed 8 d after treatment. Data are mean ± standard deviation (n = 3). (*E*) Knockout–knock-in HeLa cells expressing either wild-type (filled bars) or A776CΔ781-C (open bars) RRM1-HA were synchronized as described in the Materials and Methods. Synchronized cells were then released into G1 phase or S phase (time −3) and exposed to IR (4 Gy) 3 h after release (time 0). (*Right* panels) DNA repair was evaluated as in *A*. (*Left* panels) Cell cycle distributions are presented.

Given that levels of dNTP pools are higher during S phase than during G1 phase (Hakansson et al. 2006), recruitment of RNR at damage sites may function at a specific phase of the cell cycle where dNTP pools are low. To address this issue, we synchronized cells at S phase or G1 phase by arrest and release of thymidine or nocodazole, respectively. Recruitment of wild-type RRM1 at a DSB site was observed at both G1 and S phase (Supplemental Fig. S10). However, a comet assay revealed that A776CΔ781-C failed to rescue the impaired DNA repair in RRM1-depleted cells at G1 phase, but not at S phase (Fig. 4E). Consistently, RRM1 mutation of Tip60 binding slightly sensitizes cells to Zeocin (Supplemental Fig. S11A), which causes DNA strand breaks, but not to MMC (Supplemental Fig. S11B), which can cause interstrand cross-linking repaired mainly at S–G2 phase. Intriguingly, this G1-phase-specific impairment of DNA repair was restored when excess amounts of dADP, dGDP, dCDP, and dUMP (250 μM) were supplied in the culture medium (Supplemental Fig. S12). These results suggested that recruitment of RNR was required specifically for effective DNA repair in cells with low levels of dNTPs.

The present study suggests that the RNR recruitment to DSB sites likely provides mechanistic insights into the regulatory events that ensure a balanced supply of dNTPs during mammalian DNA repair. RNR appears to form a complex with Tip60 independently of DNA damage. Thus, it is possible that the RNR–Tip60 complex might have an alternative function, such as regulation of transcription. In response to DNA damage, regulation of the RNR subunit by Wtm1 and Dif1 in budding yeast is radically different in terms of cellular localization (Lee and Elledge 2006; Lee et al. 2008) from that observed in the present study; however, important changes in the subcellular localization of RNR might be conserved. Given that Tip60 is a key regulator of DNA damage responses, the concomitant recruitment of RNR at damage sites suggests the presence of a synthetic regulatory mechanism for DNA repair in mammals.

Materials and methods

Antibodies

Antibodies used were as follows: α-Rad51 (Ab-1, Oncogene Research Products), α-RRM1 (sc-11733 and sc-11731, Santa Cruz Biotechnologies), α-HA (11 666 606 001, Roche Applied Sciences; and PM002, MBL), α-Myc (sc-40 and sc-789, Santa Cruz Biotechnologies), α-RRM2(sc-10844, Santa Cruz Biotechnologies), α-GST (sc-459, Santa Cruz Biotechnologies), α-Chk1 (sc-8408, Santa Cruz Biotechnologies), α-IKKα (sc-7182, Santa Cruz Biotechnologies), α-Orc2 (sc-13238, Santa Cruz Biotechnologies), α-ATM (sc-23921, Santa Cruz Biotechnologies), α-ATMp1981 (no. 4526, Cell Signaling), α-acetylated histone H4 (no. 06-866, Upstate Biotechnologies), and α-phospho-histone H2AX (411-pc-020, TREVIGEN; and 05-636, Upstate Biotechnologies). Anti-Tip60 rabbit polyclonal antibodies were generated by immunization with recombinant GST-His-Tip60 produced in insect cells, and the serum obtained was affinity-purified using a GST-His-Tip60 column.

Two-hybrid interaction assays

The *pGBKT7-RRM1* plasmid was generated by insertion of the full-length human *RRM1*-encoding sequence. *pGBKT7-RRM1* was transformed into

the yeast strain AH101 and mated with yeast Y187 pretransformed with a HeLa cell cDNA library (BD Biosciences). The deletion mutants of RRM1 and Tip60 were amplified by PCR using specific sets of primers. Primer sequences are supplied in the Supplemental Material.

Affinity purification of Tip60 complex

Affinity purification of Tip60 complex was performed as described previously (Ikura et al. 2000, 2007). For the induction of DNA damage, cells were γ-irradiated (12 Gy) after centrifugation.

In situ detergent extraction and immunofluorescence analysis

Immunofluorescence on paraformaldehyde-fixed cells was performed according to a previous report (Green and Almouzni 2003), using the indicated antibodies.

Microirradiation

Microirradiation was performed as described previously (Ikura et al. 2007). In brief, GM02063 cells were maintained on the microscope stage in a Chamlide TC live-cell chamber system (Live Cell Instrument) at 37°C. Microirradiation was performed using an LSM510 confocal microscope (Carl Zeiss). Sensitization of cells was performed by incubating the cells for 20 h in medium containing 2.5 μM deoxyribosylthymine and 0.3 μM bromodeoxyuridine (Sigma), and then staining with 2 μg/mL Hoechst 33258 (Sigma) for 10 min before UVA microirradiation. The 364-nm line of the UVA laser was used for microirradiation (three pulses at 30 μW). Samples were examined with a Zeiss Axioplan 2 equipped with a charge-coupled device camera AxioCam MRm controlled by Axiovision software (Zeiss).

Knockdown experiments

HeLa cells or *STEFKu70*$^{-/-}$*phprt-DR-GFP* cells were transfected with either control siRNA (Silencer Negative Control #1, Ambion 4611), siRNAs for human Tip60 (sc-37966, Santa Cruz Biotechnologies), mouse Tip60-1 (sc-37967, Santa Cruz Biotechnologies), mouse Tip60-2 (D-057795-02-0010, Dharmacon), or RRM1 (GGAUCGCUGUCUCUAA CUUtt) using Lipofectamine 2000 reagent (Invitrogen).

Subcellular fractionation and Mnase treatment

Subcellular fractionation was performed according to a previous report (Mendez and Stillman 2000). The isolated chromatin fraction (1×10^6 cells) was treated with Mnase (15 U) for 30 min at 37°C.

Establishment of STEFKu70$^{-/-}$ *cells containing a phprt-DR-GFP cassette*

The *phprt-DR-GFP* vector (10 μg) was linearized with PvuI and transfected into *STEFKu70*$^{-/-}$ cells. Cells were selected with 1.25 μg/mL puromycin for 12 d, and single colonies were screened by Southern blotting using puromycin cDNA as a probe. Clones having only one copy of the *phprt-DR-GFP* cassette were used for experiments.

Establishment of Tet-on HeLa cells expressing NLS-RC1

pcDNA4/TO-NLS-RC1 (10 μg) was linearized with XhoI and transfected into HeLa T-Rex cells (Invitrogen). Positive clones were selected with Zeocin (250 μg/mL) and Blastcidin (5 μg/mL) for 12 d and screened by immunoblotting using anti-HA antibodies for the detection of NLS-RC1 induction in the presence of tetracycline (1 μg/mL).

Generation of adenoviruses expressing I-SceI endonuclease

The full-length *I-SceI* fragment harboring the *CAG* promoter and poly A signal was subcloned into *pAd/PL-DEST* (Invitrogen). Adenoviruses expressing I-SceI were generated according to the manufacturer's protocol (Invitrogen).

ChIP assay

A population of *STEFKu70*$^{-/-}$cells (1×10^7) containing *phprt-DR-GFP* cells infected with adenoviruses expressing I-SceI was cross-linked with 1% formaldehyde for 10 min at 37°C. ChIP assays were performed essentially as described (Shimada et al. 2008). Precipitated DNA was resuspended in 50 μL of water and analyzed by quantitative real-time PCR with the ABI PRISM7000 system using Power SYBR Green PCR Master Mix (Applied Biosystems) as described (Katsuno et al. 2009). Primers used for detection of the *I-SceI* break site were indicated in Figure 2A. As an internal control for normalization of the specific fragments amplified, mouse GAPDH locus was amplified using whole genomic DNAs with mGAPDH-F and mGAPDH-R. Primer sequences are supplied in the Supplemental Material.

Comet assay

Alkaline comet assays were performed using a Trevigen's Comet Assay kit (4250-050-k) according to the manufacturer's instructions. DNA was stained with SYBR Green, and slides were photographed digitally (Nikon Eclipse E800 lens and Fuji CCD camera). Tail moments were analyzed as reported previously (Park et al. 2006) using TriTek Comet Score Freeware.

Measurement of DNA damage sensitivity

Tet-on HeLa cells expressing NLS-RC1-HA or NLS-GFP-HA were irradiated with varying doses of IR in the presence or absence of doxycycline (1 μg/mL), and then washed with PBS. Eight days after an additional incubation, surviving colonies were counted, and their relative numbers were expressed as percentages of the untreated cells ($n = 3$).

RNR assay

Insect cells were coinfected with baculoviruses expressing wild-type RRM1 or its mutants, and with those expressing wild-type RRM2. RNR complexes were immunopurified, and their activities were determined according to a method reported previously (Fukushima et al. 2001). Amounts of wild-type RRM1 protein or its mutant proteins were determined by SDS-PAGE and used for calculating specific activities.

Cell cycle synchronization

For synchronization of cells at S phase, knockout–knock-in HeLa cells expressing wild-type or A776CΔ781-C RRM1-HA were first synchronized at the G1/S boundary by exposure to 2.5 mM thymidine for 16 h, and then released into S phase by wash-out of thymidine with PBS and the addition of 20% FBS containing DMEM. Cells were then exposed to IR 3 h after release. For synchronization of cells at G1 phase, knockout–knock-in HeLa cells were synchronized at M phase by exposure to 100 ng/mL nocodazole for 16 h and released into G1 phase by wash-out of nocodazole with PBS and addition of 20% FBS containing DMEM. Cells were then exposed to IR 3 h after release.

Acknowledgments

We thank M. Delhase for critical reading of the manuscript; M. Jasin for hprt-DR-GFP and pCBASce vectors; M. Fukushima for critical advice on the RNR assay; A. Kurimasa for *STEFKu70*$^{-/-}$ MEFs; K. Murata, C. Namikawa-Yamada, and H. Kojima for technical assistance; and M. Inagaki and H. Goto for fluorescence microscopy. This work was supported in part by the Ministry of Education, Science, Sports, and Culture of Japan through Grants-in-Aid for Scientific Research (B) (to M.N.) and (C) (to H.N.), the YASUDA Medical Foundation (to M.N.), and the Sagawa Cancer Foundation (to M.N.).

References

Dong Q, Wang TS. 1995. Mutational studies of human DNA polymerase α. Lysine 950 in the third most conserved region of α-like DNA polymerases is involved in binding the deoxynucleoside triphosphate. *J Biol Chem* **270:** 21563–21570.

Fukushima M, Fujioka A, Uchida J, Nakagawa F, Takechi T. 2001. Thymidylate synthase (TS) and ribonucleotide reductase (RNR) may be involved in acquired resistance to 5-fluorouracil (5-FU) in human cancer xenografts in vivo. *Eur J Cancer* **37:** 1681–1687.

Green CM, Almouzni G. 2003. Local action of the chromatin assembly factor CAF-1 at sites of nucleotide excision repair in vivo. *EMBO J* **22:** 5163–5174.

Guittet O, Hakansson P, Voevodskaya N, Fridd S, Graslund A, Arakawa H, Nakamura Y, Thelander L. 2001. Mammalian p53R2 protein forms an active ribonucleotide reductase in vitro with the R1 protein, which is expressed both in resting cells in response to DNA damage and in proliferating cells. *J Biol Chem* **276:** 40647–40651.

Hakansson P, Hofer A, Thelander L. 2006. Regulation of mammalian ribonucleotide reduction and dNTP pools after DNA damage and in resting cells. *J Biol Chem* **281:** 7834–7841.

Ikura T, Ogryzko VV, Grigoriev M, Groisman R, Wang J, Horikoshi M, Scully R, Qin J, Nakatani Y. 2000. Involvement of the TIP60 histone acetylase complex in DNA repair and apoptosis. *Cell* **102:** 463–473.

Ikura T, Tashiro S, Kakino A, Shima H, Jacob N, Amunugama R, Yoder K, Izumi S, Kuraoka I, Tanaka K, et al. 2007. DNA damage-dependent acetylation and ubiquitination of H2AX enhances chromatin dynamics. *Mol Cell Biol* **27:** 7028–7040.

Imaizumi T, Jean-Louis F, Dubertret ML, Bailly C, Cicurel L, Petchot-Bacque JP, Dubertret L. 1996. Effect of human basic fibroblast growth factor on fibroblast proliferation, cell volume, collagen lattice contraction: In comparison with acidic type. *J Dermatol Sci* **11:** 134–141.

Johnson RE, Trincao J, Aggarwal AK, Prakash S, Prakash L. 2003. Deoxynucleotide triphosphate binding mode conserved in Y family DNA polymerases. *Mol Cell Biol* **23:** 3008–3012.

Katsuno Y, Suzuki A, Sugimura K, Okumura K, Zineldeen DH, Shimada M, Niida H, Mizuno T, Hanaoka F, Nakanishi M. 2009. Cyclin A–Cdk1 regulates the origin firing program in mammalian cells. *Proc Natl Acad Sci* **106:** 3184–3189.

Kraynov VS, Showalter AK, Liu J, Zhong X, Tsai MD. 2000. DNA polymerase β: Contributions of template-positioning and dNTP triphosphate-binding residues to catalysis and fidelity. *Biochemistry* **39:** 16008–16015.

Lee YD, Elledge SJ. 2006. Control of ribonucleotide reductase localization through an anchoring mechanism involving Wtm1. *Genes & Dev* **20:** 334–344.

Lee YD, Wang J, Stubbe J, Elledge SJ. 2008. Dif1 is a DNA-damage-regulated facilitator of nuclear import for ribonucleotide reductase. *Mol Cell* **32:** 70–80.

Mendez J, Stillman B. 2000. Chromatin association of human origin recognition complex, cdc6, and minichromosome maintenance proteins during the cell cycle: Assembly of prereplication complexes in late mitosis. *Mol Cell Biol* **20:** 8602–8612.

Murr R, Loizou JI, Yang YG, Cuenin C, Li H, Wang ZQ, Herceg Z. 2006. Histone acetylation by Trrap–Tip60 modulates loading of repair proteins and repair of DNA double-strand breaks. *Nat Cell Biol* **8:** 91–99.

Niida H, Katsuno Y, Banerjee B, Hande MP, Nakanishi M. 2007. Specific role of Chk1 phosphorylations in cell survival and checkpoint activation. *Mol Cell Biol* **27:** 2572–2581.

Nordlund P, Reichard P. 2006. Ribonucleotide reductases. *Annu Rev Biochem* **75:** 681–706.

Park JH, Park EJ, Lee HS, Kim SJ, Hur SK, Imbalzano AN, Kwon J. 2006. Mammalian SWI/SNF complexes facilitate DNA double-strand break repair by promoting γ-H2AX induction. *EMBO J* **25:** 3986–3997.

Pierce AJ, Hu P, Han M, Ellis N, Jasin M. 2001. Ku DNA end-binding protein modulates homologous repair of double-strand breaks in mammalian cells. *Genes & Dev* **15:** 3237–3242.

Pontarin G, Fijolek A, Pizzo P, Ferraro P, Rampazzo C, Pozzan T, Thelander L, Reichard PA, Bianchi V. 2008. Ribonucleotide reduction is a cytosolic process in mammalian cells independently of DNA damage. *Proc Natl Acad Sci* **105:** 17801–17806.

Reichard P. 1993. From RNA to DNA, why so many ribonucleotide reductases? *Science* **260:** 1773–1777.

Shimada M, Niida H, Zineldeen DH, Tagami H, Tanaka M, Saito H, Nakanishi M. 2008. Chk1 is a histone H3 threonine 11 kinase that regulates DNA damage-induced transcriptional repression. *Cell* **132:** 221–232.

Zhang Z, Yang K, Chen CC, Feser J, Huang M. 2007. Role of the C terminus of the ribonucleotide reductase large subunit in enzyme regeneration and its inhibition by Sml1. *Proc Natl Acad Sci* **104:** 2217–2222.

Biochemical and Biophysical Research Communications 380 (2009) 460–466

Contents lists available at ScienceDirect

Biochemical and Biophysical Research Communications

journal homepage: www.elsevier.com/locate/ybbrc

Ptpcd-1 is a novel cell cycle related phosphatase that regulates centriole duplication and cytokinesis

Doaa H. Zineldeen, Midori Shimada, Hiroyuki Niida, Yuko Katsuno, Makoto Nakanishi *

Department of Cell Biology and Biochemistry, Graduate School of Medical Sciences, Nagoya City University, 1 Kawasumi, Mizuho-cho, Mizuho-ku, Nagoya 467-8601, Japan

ARTICLE INFO

Article history:
Received 6 January 2009
Available online 24 January 2009

Keywords:
Centrosome
Phosphatase
Mitosis
Polo-like kinases
Cytokinesis
Cdc14

ABSTRACT

Proper progression of mitosis requires spatio-temporal regulation of protein phosphorylation by orchestrated activities of kinases and phosphatases. Although many kinases, such as Aurora kinases, polo-like kinases (Plks), and cyclin B-Cdk1 are relatively well characterized in the context of their physiological functions at mitosis and regulation of their enzymatic activities during mitotic progression, phosphatases involved are largely unknown. Here we identified a novel protein tyrosine phosphatase containing domain 1 (Ptpcd 1) as a mitotic phosphatase, which shares sequence homology to Cdc14. Immunofluorescence studies revealed that Ptpcd1 partially colocalized with γ-tubulin, an archetypical centrosomal marker. Overexpression of this phosphatase prevented unscheduled centrosomal amplification in hydroxyurea arrested U2OS cells. Intriguingly, Ptpcd 1-associated and colocalized with polo-like kinase 1(Plk1). Hence, overexpression of Ptpcd1 rescued prometaphase arrest of Plk-1 depleted cells, but resulted in aberrant cytokinesis as did as Plk1 overexpression. These results suggested that Ptpcd1 is involved in centrosomal duplication and cytokinesis.

Faithful transmission of genetic information relies on the coordinated regulatory system of the cell cycle [1]. In higher eukaryotes, mitosis involves many dynamic processes at chromosomes, including condensation and segregation, both of which are mainly regulated by protein phosphorylation and dephosphorylation [2]. Proper segregation of chromosomes requires centrosomal maturation, separation, spindle formation and alignment of chromosomes [2,3]. Centrosome is the major microtubule organizing center in animal cells composed of two centrioles, which are barrel shaped structures with nine triple microtubules and a pericentriolar matrix responsible for nucleating microtubules and organizing mitotic spindles for bipolar separation of sister chromatids [4,5]. The identification of several centrosome-associated protein kinases has proposed the concept that multiple regulatory phosphorylation pathways tightly control centrosome cycle during cell cycle [6–8]. Around G1/S transition, a procentriole forms adjacent to each parental centriole and continues growing during S phase. At the onset of mitosis, the two centrosomes separate and the daughter centriole matures and instructs mitotic spindle formation [4]. In post-mitotic cells, centrosome migrates to the cell surface and one of the centrioles differentiates into a basal body that nucleates microtubules to form a cilium [5].

Polo-like kinases (Plks) regulate a multitude of several mitotic processes, including centrosome duplication, maturation [9], bipolar spindle formation [10], microtubule/kinetochore interactions, and cytokinesis [11,12]. Spatio-temporal coordination of Plks activities is achieved through binding to phosphorylated docking proteins with distinct subcellular localizations, such as centrosomes, kinetochore, and the midzone [12,13]. At early mitosis, Cdk1 creates the phosphorylated docking sites on the substrates [1], whereas Plks create their own docking sites on other partners after inactivation of Cdk1 [1,12,13]. In budding yeast, some parts of mitotic function of Plks appear to be mediated by Cdc14p. Cells lacking Cdc14p are unable to exit from mitosis, with defects in both movement of chromosomes to the spindle poles and elongation of anaphase spindles [14]. Mammalian cells possess two Cdc14 paralogue, Cdc14A and Cdc14B, identified based on their sequence similarity to Cdc14p [15]. Recent studies suggested that Cdc14A and Cdc14B might be involved in distinctive cellular functions; the former functioned in centrosomal separation and cytokinesis [3,16], and the latter in centrosomal duplication and microtubule stabilization [17]. However, Cdc14B deficient cells were viable and lacked apparent defects in chromosome segregation and cytokinesis [18], suggesting that alternative phosphatase(s) might be capable of complementing the mitotic functions of Cdc14B. Here, we identified Ptpcd1 as a possible functional isozyme of mammalian Cdc14B that is genetically linked to Plk1.

Materials and methods

Cloning of Ptpcd1. The complete ORF of Ptpcd1 (corresponding exactly to AW456874; No. NM 207232 and MGI: 2145430) was

* Corresponding author. Fax: +81 52 842 3955.
E-mail address: mkt-naka@med.nagoya-cu.ac.jp (M. Nakanishi).

0006-291X/$ - see front matter © 2009 Elsevier Inc. All rights reserved.
doi:10.1016/j.bbrc.2009.01.113

amplified by PCR using mouse brain cDNA library as a template with the following primer set: 5′-ATG GCG CAG GAG TCT TGC CA-3′ and 5′-TCA GGA GAG GCT GCT GTC CTT TTT GC-3′. The PCR product was subcloned into pCR II-TOPO (Invitrogen). pcDNA3.1-Myc/HisPtpcd1 was then generated by subcloning of the KpnI/NotI fragment into pcDNA3.1Myc/His vector. The KpnI/NotI fragment was amplified by PCR using pCRII-TOPOPtpcd1 as a template with a set of primers; 5′-TTT GAA TTC GCC ACC ATG TCG TCC GGG GCC AAG GAG-3′and 5′-AAA TCT AGA GGG CAG AGG GGT CCC GTT-3′. pcDNA3.1Plk1-HA was generated by subcloning of EcoRI/NotI fragment from pET23d-Plk1 (kind gift from Dr. Nishida) into pcDNA3.1HA.

Cell culture. HeLa and U2OS cells were cultured and maintained in Dulbecco's modified Eagle's medium (Invitrogen) supplemented with 10% fetal bovine serum as described previously [19]. Nocodazole and hydroxyurea were purchased from Sigma.

Knockdown experiments. Plasmid transfections were performed using FuGENE6 transfection reagent (Roch) according to manufacturer's instruction. Stealth siRNAs for Plk1 (Invitrogen) or control (Invitrogen) were transfected using lipofectamin 2000 (Invitrogen).

Immunoblotting. Antibodies used in this study were anti-c-myc (sc-789; Santa Cruz, sc-40; Santa Cruz), anti-pTyr-Cdk1 (9111; Cell signaling), anti-cyclin B1 (GNS1; Santa Cruz), anti-Plk1 (35-200; upstate), anti-HA (12CA5; Roch), anti-γ-tubulin (T3559; Sigma) and anti-α-tubulin (Sigma). Whole cell extracts were prepared as described previously [20] and were subjected to immunoblotting. For IP-immunoblotting, U2OS cells were cotransfected with Plk1-HA, along with Ptpcd1-myc or empty pcDNA3.1. Cells were harvested in RIPA buffer (10 mM Tris–HCl, pH7.5, 150 mM NaCl, 0.5% Triton X-100, 1% sodium deoxycholate and complete protease inhibitor tablets (1/10 ml) (Roch). The lysates (200 μg) were incubated with anti-myc antibodies (5 μg) or mouse normal IgG as a control at 4 °C for 1 h and then precipitated with 20 μl of protein G beads. The resultant precipitates were separated by SDS–PAGE and then analyzed by immunoblotting.

Microtubule regrowth assay. Cells on coverslips were treated with 4 mM nocodazole for 30 min at 37 °C, followed by replacement with normal medium. Cells were fixed at −20 °C with methanol and immunostained for immunofluorescence microscopy was performed as described previously [21].

Immunofluorescence analysis. Secondary antibodies for immunofluorescence microscopy were Cy3 (Jackson immunoresearch), Alexa 594 and Alexa 488 (Molecular probes). Cells on coverslips were fixed in 4% PFA for 10 min at RT and then permeabilized with 0.25% Triton X-100 in PBS. Blocking was done in 5% normal goat serum (Convac) containing 1% Triton X-100. Fixed cells were incubated with antibodies in blocking for 1 h at RT. DNA was counterstained with DAPI (2 mg/ml). For centrosomal staining, cells were fixed with methanol at −20 °C for 10 min.

Results and discussion

Ptpcd 1 is a centrosomal phosphatase that regulates centrosomal duplication during S phase

Immotile primary cilium is a centriole-based organelle that consists of microtubule pairs located at the plasma membrane [22]. The fact that a cilium is differentiated from centrosomes after mitosis has suggested that the function and structures of cilia are regulated by similar mechanisms to those of centrosomes [23]. Indeed, Nek2 and Aurora A kinases are involved in the regulation of both centrosomes and cilia functions [24]. Ptpcd 1 was originally identified as a dual specificity protein phosphatase highly expressed in mouse cilia [25]. We therefore speculated that Ptpcd 1 might be involved in the regulation of centrosomal function. Ptpcd 1 encodes a 721 amino acid protein with a predicated molecular weight of 82 kDa. Sequence analysis of Ptpcd1 revealed the significant homology with yeast Cdc14p with coiled coil domain at its carboxyl terminal, RXXL motif (a putative APC/C binding motif), several nuclear localization signals (Suppl. Fig. 1A), and a putative nuclear export signal (Suppl. Fig. 1B). To examine whether Ptpcd1 functions at centrosomes, Ptpcd1-myc was transfected into HeLa cells. In interphase cells, signals corresponding to Ptpcd1 were detected at both cytoplasm and nucleus with one or two closely spaced dots. Importantly, these dot signals were localized adjacent to, but not overlapped with, the signals from γ-tubulin, a centrosomal protein, raising the possibility of its centriolar localization (Fig. 1A). This centrosomal enrichment of Ptpcd1 was observed from interphase to anaphase, whereas it was hardly detected at telophase where most of the immunoreactivity was detected at midbody. This spatio-temporal localization in relation to cell cycle conveyed that Ptpcd1 might be a novel centrosomal-related phosphatase.

In certain transformed cells, such as U2OS cells, prolonged S phase arrest by hydroxyurea (HU) causes uncoupled centrosomal duplication from cell cycle with multiple rounds of centriole duplication in the absence of DNA replication and mitotic division (Fig. 1B, upper panel) [15]. In order to examine whether Ptpcd-1 plays a role in the regulation of centriole duplication, Ptpcd1 were overexpressed into U2OS cells in the presence of 4 mM HU for 72 h. Ptpcd 1 expression inhibited HU-induced centriole over duplication (Fig. 1B, lower panel). Majority of control U2OS cells possessed more than single centrosome when cells were treated with HU. In contrast, 60% of Ptpcd 1 expressing cells possessed single centrosome (Fig. 1C). These results clearly indicated that overexpression of Ptpcd1 suppressed uncoupled centrosomal duplication during S phase. Given that Cdk activity regulates centrosomal duplication during S phase, we asked whether Ptpcd1 affect inhibitory phosphorylation of Cdc2 at Y15, which is regulated at centrosomes during S to G2 phase. Cdc2 phosphorylation at Y15 slightly decreased, whereas expression of cyclin B1 was not affected by Ptpcd1 expression (Fig. 1D).

Ptpcd1 associates with Plk1 and is involved in the regulation of mitotic progression

Plk1 regulates centrosomal functions at multiple levels, such as centrosomal stabilization, nucleation, duplication, microtubule stabilization, and cytokinesis [9–13]. Therefore, Ptpcd1 might be involved in Plk1-dependent regulation of centrosome functions. To examine this possibility, we first asked whether Ptpcd1 physically interact with Plk1. Plk1-HA and Ptpcd1-myc were co-transfected into HeLa cells and the cell extracts were immunoprecipitated with anti-myc antibodies. Plk1-HA as well as Ptpcd1-myc was readily detected in the myc-immunoprecipitates, indicating that Plk1-HA was capable of forming a complex with Ptpcd1-myc (Fig. 2A). Immunocytochemical analysis revealed colocalization of ectopically expressed Ptpcd1-myc with endogenous Plk1 (Fig. 2B). Intriguingly, Ptpcd1-myc appeared to accumulate and colocalize with Plk1 at mid-body in telophase cells. These results suggested that Ptpcd1 might also function in cytokinesis as Plk1 did [1]. To address this question, we examined the effect of Ptpcd1 overexpression on mitotic progression. Aberrant cytokinesis in the form of fused or intercellular α-tubulin bridges was apparent in cells expressing Ptpcd1 (Fig. 3A and C). Hence, an increase in the number of cells with multiple nuclei was observed when Ptpcd1 was overexpressed (Fig. 3B and C). These results suggested that Ptpcd1 as well as Plk1 as reported played an important role in cytokinesis.

In addition to cytokinesis, Plk1 was reported to stabilize microtubule organization [10,12]. Therefore, we then asked if Ptpcd1 expression affect the microtubule stabilization. HeLa cells were transfected with pcDNA3.1Ptpcd1-myc and treated with nocodaz-

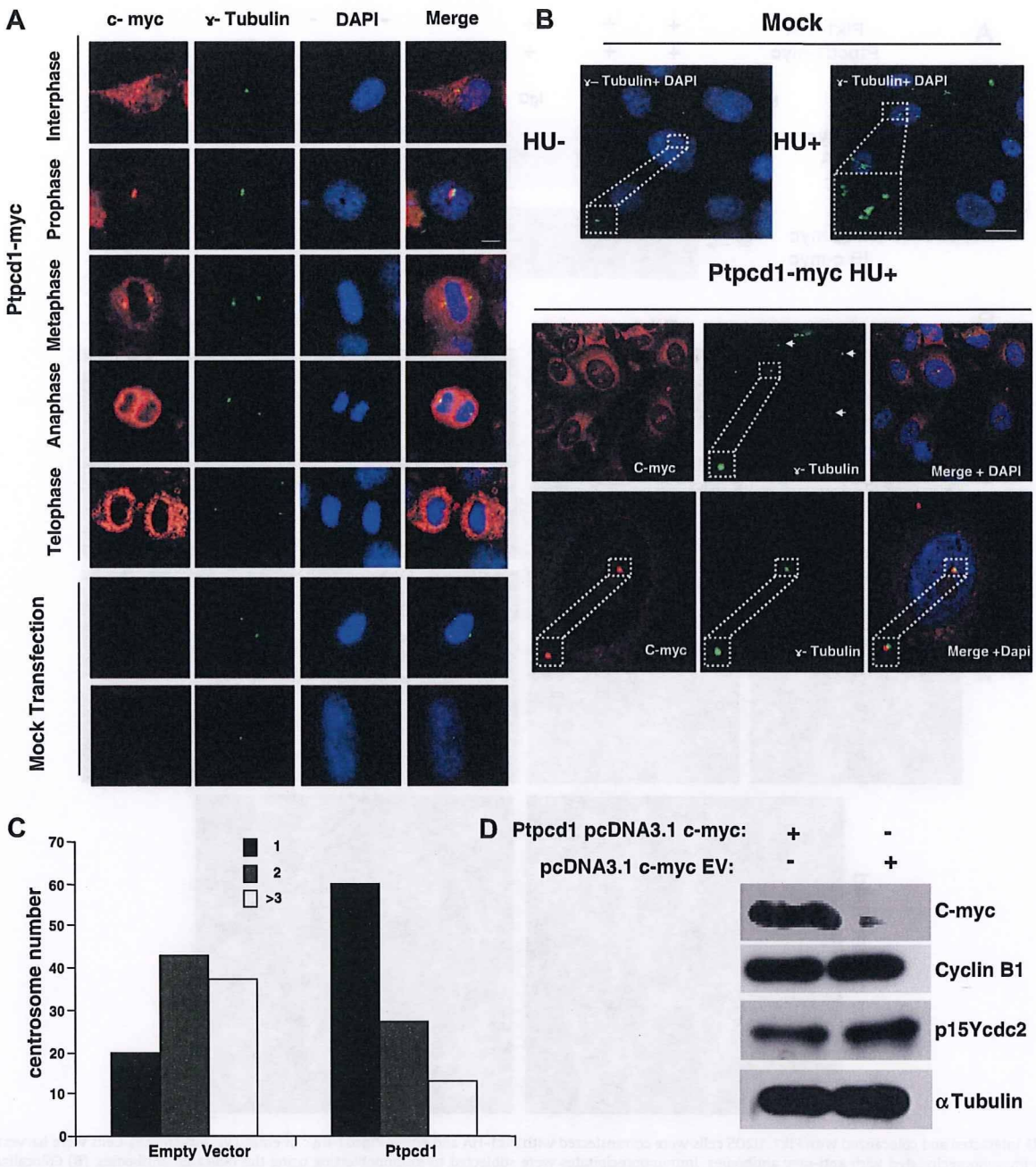

Fig. 1. Ptpcd1 localized to centrosomes and its overexpression prevents unscheduled centriole duplication. (A) Either Ptpcd1-myc or empty pcDNA3.1 as a negative control was transfected into HeLa cells. Cells were fixed with methanol and co-immunostained with γ-tubulin (green) and c-myc (red). DNA was counterstained with DAPI (blue). Scale bars; 5 μm. (B) Overexpression of Ptpcd1 prevents unscheduled centriole duplication. U2OS cells were transfected with either empty vector the presence or absence of HU (4 mM). (upper panels) or Ptpcd1-myc (lower panels) in the presence of HU (4 mM). Cells were then fixed and immunostained with anti-γ-tubulin antibodies (green) and c-myc (red). Arrows point at centrosomes, enlarged insets showed centrosomes. Scale bars; 5 μm. (C) The number of cells with 1, 2, or more than 2 centrosomes from (B) was counted and shown as a percentage of total cells. (D) Immunoblotting analysis. Whole cell extracts from (B) were subjected to immunoblotting using the indicate antibodies. (For interpretation of color mentioned in this figure the reader is referred to the web version of the article.)

ole, a microtubule depolymerizing agent. Overexpression of Ptpcd1-myc significantly stabilized microtubule organization when it was evaluated by staining with α-tubulin (Fig. 3D). Interestingly, it also enhanced microtubule regrowth after nocodazole washout. Thus, the effect of Ptpcd1-myc expression on microtubules stabilization was similar to that of Plk1 expression, further suggesting that Ptpcd1 functioned in Plk1-regulatory networks. In addition, these results also showed that the centrosomal localization of Ptpcd1 was independent of microtubules nucleation because centrosomal signals of Ptpcd1 could still be detected after microtubules depolymerization with nocodazole.

Overexpression of Ptpcd1 is capable of complementing prometaphase arrest in Plk1 depleted cells

We finally determined the genetic orientation between Plk1 and Ptpcd1. Endogenous Plk1 was depleted by the transfection of the specific siRNAs (D-1 and D-2) for Plk1. Immunoblotting using

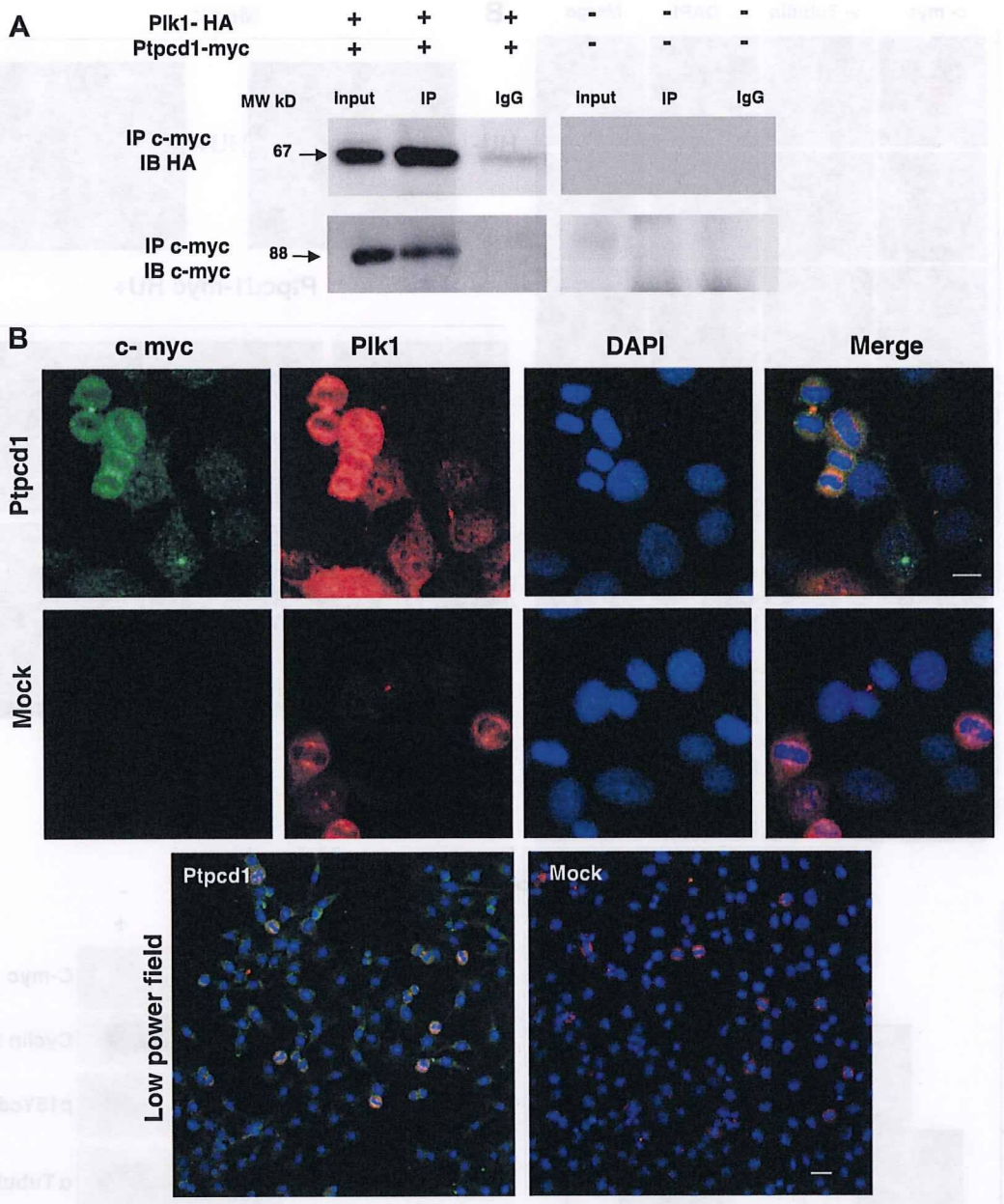

Fig. 2. Ptpcd1 interacted and colocalized with Plk1. U2OS cells were cotransfected with Plk1-HA and either Ptpcd1-myc or empty vectors (mock). Cells were harvested, and lysates were immunoprecipitated with anti-myc antibodies. Immunoprecipitates were subjected to immunoblotting using the indicated antibodies. (B) Colocalization of Ptpcd1 with Plk1. U2OS cells were transfected with Ptpcd1-myc and then stained with anti-myc antibodies (green) and anti-Plk1 antibodies (red, upper panels). DNA was counterstained with DAPI. Lower panels were low power fields of the upper images. Scale bars; 5 μm. (For interpretation of color mentioned in this figure the reader is referred to the web version of the article.)

anti-Plk1 antibodies revealed that transfection of D-1 and D-2 resulted in a significant reduction in Plk1 protein, whereas that of control siRNA did not (Fig. 4A). Plk1 depletion results in prometaphase/metaphase arrest [1], presumably due to impaired centrosomal separation, centrosome fragmentation, and microtubules destabilization, which consequently activate spindle checkpoints. Prolonged prometaphase arrest in Plk1 depleted cells ultimately appeared to induce apoptosis (Fig. 4B and Suppl. Fig. 2). Intriguingly, ectopic expression of Ptpcd1 in Plk1 depleted cells rescued the prometaphase/metaphase arrest and stabilized microtubules (Suppl. Fig. 2), but resulted in aberrant cytokinesis as was observed in Ptpcd1 expressing cells (Fig. 3C). These results indicated that Ptpcd1 at least in part functioned downstream of Plk1. Consistent with this notion, Ptpcd1 possessed four consensus serine residues for a Plk1 phosphorylation site (Fig. 4C) [26]. In this regard, Cdc5, a yeast homolog of Plks, regulated Cdc14p phosphorylation and its subcellular localization to ensure mitotic exit [14,27].

In summary, based on our observation in this study, it is possible that Ptpcd1 together with Plk1 may regulate the centriole duplication cycle as well as cytokinesis by modulating the phosphorylation status of some proteins, suggesting the conserved mechanism from yeast to mammalian by which Cdc5–Cdc14 axis regulates mitotic exit [1,14,27]. A similar counterbalance of kinase and phosphatase activities was also proposed in Nek2 and PP1α

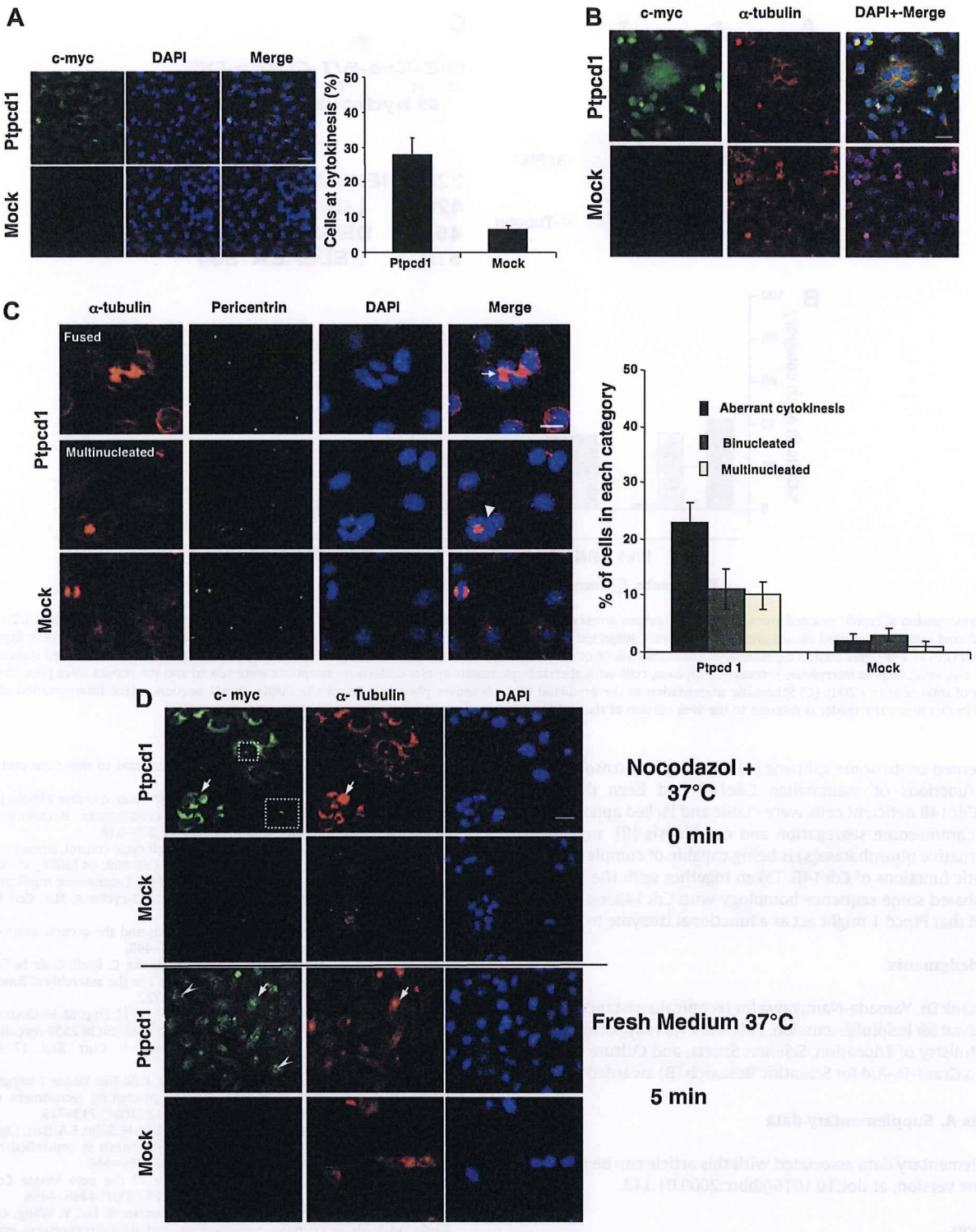

Fig. 3. Overexpression of Ptpcd1 resulted in aberrant cytokinesis and microtubules stabilization. (A) HeLa cells were transfected with either Ptpcd1-myc or empty vector (mock). Cells were immunostained with anti-myc (green) and DNA was counterstained with DAPI (blue). Scale bars; 5 μm (left panel). Cells with cytokinesis were counted and the data were presented as a percentage of total cells ($n > 200$) and means ± SD from three independent experiments (right panel). (B) HeLa cells were transfected as in (A) and stained with the indicated antibodies. DNA was counterstained with DAPI. (C) HeLa cells were transfected as in (B) and immunostained with anti-tubulin (red) and pericentrin (green). DNA was counterstained with DAPI. White arrow indicated persistent midbody structure and arrowhead pointed at multinucleated cells (left panels). Scale bars; 5 μm. Cells with aberrant cytokinesis, binucleated, and multinucleated cells from (left panels) were counted and the data were presented as a percentage of total cells ($n > 100$) and means ± SD from three independent experiments. (D) Microtubule regrowth assay. HeLa cells were transfected with either pcDNA3.1Ptpcd1-myc or empty vector. Cells were then treated with nocodazole as in Materials and Methods, and stained with anti-myc (green) and anti-α-tubulin (red) antibodies (upper panels). Cells were further cultured with the medium in the absence of nocodazole for 5 min and then stained as described above (lower panels). White arrow indicated stabilized α-tubulin bundles by Ptpcd1 and arrow head indicated newly growing microtubules. Insets show centrosomal Ptpcd1, Scale bars; 5 μm. (For interpretation of color mentioned in this figure the reader is referred to the web version of the article.)

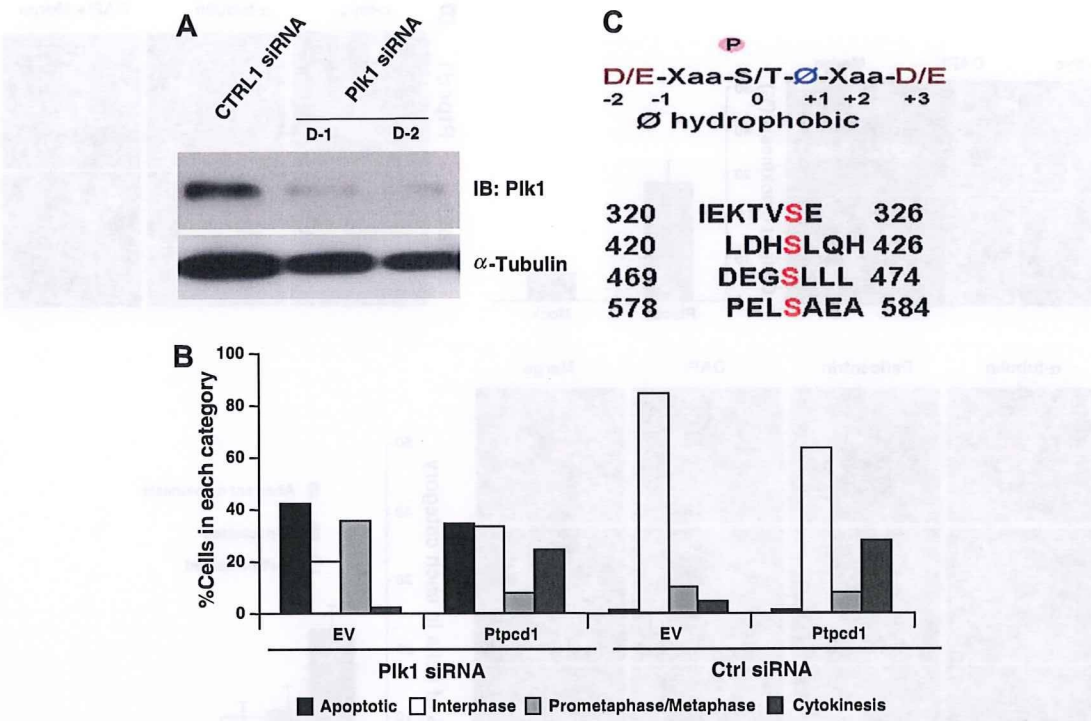

Fig. 4. Overexpression of Ptpcd1 rescued prometaphase/metaphase arrest observed in Plk1 depleted cells. (A) Plk1 depletion by transfection of its specific siRNAs. U2OS cells were transfected with the indicated siRNAs and the lysates were subjected to immunoblotting using the indicated antibodies. (B) U2OS cells were transfected with Ptpcd1 or empty vector (EV) as a negative control together with either Plk1 siRNA or control siRNA as indicated. The transfected cells were then fixed and immunostained stained with c-myc and α-tubulin. Cells in interphase, prometa/metaphase, cells with aberrant cytokinesis and/or underwent apoptosis were scored and the results were presented as a percentage of total cells ($n > 200$). (C) Schematic presentation of the predicted plk1 consensus phosphorylation site inside Ptpcd1 sequence. (For interpretation of color mentioned in this figure the reader is referred to the web version of the article.)

that governed centrosome splitting [4]. Although centrosomal and mitotic functions of mammalian Cdc14B had been described [15,17], Cdc14B deficient cells were viable and lacked apparent defects in chromosome segregation and cytokinesis [8], suggesting that alternative phosphatase(s) is being capable of complementing the mitotic functions of Cdc14B. Taken together with the fact that Ptpcd1 shared some sequence homology with Cdc14B, our results proposed that Ptpcd 1 might act as a functional isozyme to Cdc14B.

Acknowledgments

We thank Dr. Yamada-Namikawa for technical assistance and Dr. Majid Safwat for helpful discussion. This work was supported in part by the Ministry of Education, Science, Sports, and Culture of Japan through a Grant-in-Aid for Scientific Research (B) awarded to M.N.

Appendix A. Supplementary data

Supplementary data associated with this article can be found, in the online version, at doi:10.1016/j.bbrc.2009.01.113.

References

[1] T. Takaki, K. Trenz, V. Costanzo, M. Petronczki, Polo-like kinase 1 reaches beyond mitosis—cytokinesis, DNA damage response, and development, Curr. Opin. Cell Biol. 6 (2008) 650–660.
[2] L. Trinkle-Mulcahy, A.I. Lamond, Mitotic phosphatases: no longer silent partners, Curr. Opin. Cell Biol. 18 (2006) 623–631.
[3] K. Yuan, H. Hu, Z. Guo, G. Fu, A.P. Shaw, R. Hu, X. Yao, Phospho-regulation of HsCdc14A By polo-like kinase 1 is essential for mitotic progression, J. Biol. Chem. 282 (2007) 27414–27423.
[4] P. Meraldi, E.A. Nigg, Centrosome cohesion is regulated by a balance of kinase phosphatase activities, J. Cell Sci. 114 (2001) 3749–3757.
[5] C.G. Pearson, B.P. Culver, M. Winey, Centrioles want to move out and make cilia, Dev. Cell 13 (2007) 319–321.
[6] N. R Helps, X. Luo, H.M. Barker, P.T. Cohen, NIMA-related kinase 2 (Nek2), a cell cycle-regulated protein kinase localized to centrosomes, is complexed to protein phosphatase 1, Biochem. J. 349 (2000) 509–518.
[7] B.M. Lange, Integration of the centrosome in cell cycle control, stress response and signal transduction pathways, Curr. Opin. Cell Biol. 14 (2002) 35–43.
[8] P. Meraldi, J. Lukas, A.M. Fry, J. Bartek, E.A. Nigg, Centrosome duplication in mammalian somatic cells requires E2F and Cdk2-cyclin A, Nat. Cell Biol. 1 (1999) 88–93.
[9] F.A. Barr, H.H. Sillje, E.A. Nigg, Polo-like kinases and the orchestration of cell division, Nat. Rev. Mol. Cell Biol. 5 (2004) 429–440.
[10] I. Sumara, J.F. Gimenez-Abian, D. Gerlich, T. Hirota, C. Kraft, C. de la Torre, J. Ellenberg, J.M. Peters, Roles of polo-like kinase 1 in the assembly of functional mitotic spindles, Curr. Biol. 14 (2004) 1712–1722.
[11] P. Lenart, M. Petronczki, M. Steegmaier, B. Di Fiore, J.J. Lipp, M. Hoffmann, W.J. Rettig, N. Kraut, J.M. Peters, The small molecule inhibitor BI 2536 reveals novel insights into mitotic roles of polo-like kinase 1, Curr. Biol. 17 (2007) 304–315.
[12] M. Petronczki, M. Glotzer, N. Kraut, J.M. Peters, Polo-like kinase 1 triggers the initiation of cytokinesis in human cells by promoting recruitment of the RhoGEF Ect2 to the central spindle, Dev. Cell 12 (2007) 713–725.
[13] R. Neef, U. Gruneberg, R. Kopajtich, X. Li, E.A. Nigg, H. Sillje, F.A. Barr, Choice of Plk1 docking partners during mitosis and cytokinesis is controlled by the activation state of Cdk1, Nat. Cell Biol. 9 (2007) 436–444.
[14] R. Visintin, F. Stegmeier, A. Amon, The role of the polo kinase Cdc5 in controlling Cdc14 localization, Mol. Biol. Cell 14 (2003) 4486–4498.
[15] J. Wu, H.P. Cho, D.B. Rhee, D.K. Johnson, J. Dunlap, Y. Liu, Y. Wang, Cdc14B depletion leads to centriole amplification, and its overexpression prevents unscheduled centriole duplication, J. Cell Biol. 181 (2008) 475–483.
[16] B.K. Kaiser, Z.A. Zimmerman, H. Charbonneau, P.K. Jackson, Disruption of centrosome structure, chromosome segregation, and cytokinesis by misexpression of human Cdc14A phosphatase, Mol. Biol. Cell 13 (2002) 2289–2300.
[17] H.P. Cho, Y. Liu, M. Gomez, J. Dunlap, M. Tyers, Y. Wang, The dual-specificity phosphatase CDC14B bundles and stabilizes microtubules, Mol. Cell Biol. 25 (2005) 4541–4551.
[18] E. Berdougo, M.V. Nachury, P.K. Jackson, P.V. Jallepalli, The nucleolar phosphatase Cdc14B is dispensable for chromosome segregation and mitotic exit in human cells, Cell Cycle 7 (2008) 1184–1190.